PCCP

Research Progress on Surface Modifications for Phosphors Used in Light-Emitting Diodes (LEDs)

Journal:	*Physical Chemistry Chemical Physics*
Manuscript ID	CP-REV-04-2023-001658.R1
Article Type:	Review Article
Date Submitted by the Author:	05-Aug-2023
Complete List of Authors:	ZHANG, Chenning; Hosei University, Department of Chemical Science and Technology; National Institute for Materials Science Uchikoshi, Tetsuo; National Institute for Materials Science, Research Center for Functional Materials Takeda, Takashi; National Institute for Materials Science, Hirosaki, Naoto; National Institute for Materials Science, Nano Ceramics Center

ARTICLE

Research Progress on Surface Modifications for Phosphors Used in Light-Emitting Diodes (LEDs)

Received 00th January 20xx,
Accepted 00th January 20xx

DOI: 10.1039/x0xx00000x

Chenning Zhang,*[a b] Tetsuo Uchikoshi,[b] Takashi Takeda,[b] and Naoto Hirosaki[b]

Stable and efficient phosphors are highly important for light-emitting diodes (LEDs) with respect to their application in solid-state lighting, instead of conventional lamps for general lighting. However, some problems, like low stability, low photoluminescence (PL) efficiency, and serious thermal degradation, are commonly encountered in the phosphors for limiting their applications in LEDs. Surface modification for some phosphors commonly-used in LEDs lighting, including fluoride, sulphide, silicate, oxide, nitride, and oxynitride phosphors are presented in this review. By forming protective surface layer, the stabilities against moisture and high temperature of fluorides-and sulphides-based phosphors were strengthened; by coating inorganic and organic materials around the particle surface, the PL efficiencies of silicates-and oxides-based phosphors were improved; by passivation treatment upon the phosphor surface, the thermal degradation of nitrides-and oxynitrides-based phosphors were reduced. Various technologies for the surface modification are described in detail, moreover, the mechanisms about stability strengthening, PL efficiency improvement, and thermal degradation reduction are explained. In addition, embedding phosphors in inorganic glass matrix, especially for quantum dots (QDs), are also introduced as an effective method to improve phosphor stability for LED applications. Finally, the future development of surface modification on phosphors are proposed.

Introduction

Light-emitting diodes (LEDs) as solid-state lighting is an emerging technology with potentially exceeding traditional lamp-based lighting systems.[1] The operation of LEDS is based on spontaneous light emission in semiconductors with small energy losses in injection current. As a result, comparing with conventional lamps, the light sources based on LEDs have superior energy savings, environment-friendliness, small volume, and long persistence, therefore significantly reducing the power consumption and pollution from fossil fuel power plants.[2] Currently, LEDs have been widely used in applications of indicators, decorated lamps, backlights of liquid crystal displays, and plant lightings. In the near future, with the development of LEDs, it would replace conventional lamps for general lighting.[3]

According to three methods of creating white light in LEDs, appropriate phosphors are used as down-conversion luminescent materials. Moreover, the phosphors used in LEDs should not only have high absorption of ultra-violet (UV) or blue light, but also have some characteristics including high conversion efficiency, high stability against chemicals and moisture, low thermal quenching, and appropriate emission colours.[4] Generally, the phosphors most commonly used in LEDs are fluorides, sulphides, silicates, oxides, nitrides, and oxynitrides. However, some problems are found in these phosphors for limiting their applications in LEDs, that is, fluorides-and sulphides-based phosphors are very sensitive to moisture, making luminescent intensity dramatically degrade;[5–7] silicates-and oxides-based phosphors have low emission efficiency and so are difficultly used for high-efficiency LEDs;[8–11] and nitrides-and oxynitrides-based phosphors have serious thermal degradation,[2, 12–14] which cause short life time for the LEDs device.

Comparing with tailoring crystal structure of phosphor host, the methods of treatment upon particle surface are considered as facial ways to solve the problems mentioned above. In this review, recent developments and research reports concerning about coating protective layer and surface modification are typically discussed for the phosphors including fluorides, sulphides, silicates, oxides, nitrides, and oxynitrides.

Phosphors used for LEDs with surface modification

Fluoride phosphors

Mn^{4+}-activated red-emitting fluoride phosphors with promising narrow-band and high luminescent efficiency are indispensable candidates for LEDs, however, their poor moisture resistance and fluorescent thermal stability are the main obstacles for such phosphors in practical applications.[15–17] Several methods of surface

[a] Department of Chemical Science and Technology, Hosei University, Koganei, Tokyo 184-8584, Japan. E-mail: zhang.chenning2015@gmail.com
[b] Research Center for Electronic and Optical Materials, National Institute for Materials Science, Tsukuba, Ibaraki 305-0047, Japan. E-mail: zhang.chenning@nims.go.jp

† Footnotes relating to the title and/or authors should appear here.
Electronic Supplementary Information (ESI) available: [details of any supplementary information available should be included here]. See DOI: 10.1039/x0xx00000x

modification were employed for improving their stabilities by forming a protective coating layer around particle surface.

A new class of Mn^{4+}-doped A_2MF_6 (A = Li, Na, and K; M = Si and Ti) fluoride phosphors has attracted increasing attention as red components because of their excellent optical properties, including narrow-band emission within the spectral sensitivity of human eye, high luminous efficiency, and excellent colour rendering indices (80–86).[18, 19] With unique and efficient narrow-band red emission and broadband blue light absorption characteristics, Mn^{4+}-activated fluoride red phosphors have gained increasing attention in warm WLEDs and liquid crystal display (LCD) backlighting applications,[20–22] whereas the intrinsic hygroscopic nature of these phosphors has inevitably limited their practical applications.[23, 24] Despite their exceptional luminescent properties, sensitivity to atmospheric moisture has limited their applications. P. Arunkumar et al.,[25] prepared a form a metal-free, organic, passivating skin using oleic acid (OA) as a hydrophobic encapsulant for red-emitting fluoride phosphor of $K_2SiF_6:Mn^{4+}$ by solvothermal treatment. The OA-passivated $K_2SiF_6:Mn^{4+}$ (KSF-OA) phosphor exhibited the unique property of stable emission efficiency by controlling thickness and highly transparent passivating layer. Meanwhile, the KSF-OA phosphor exhibited excellent moisture stability and maintained 85% of its emission intensity even after 450 h at high temperature (85°C) and humidity (85%). Emission spectra of pristine KSF and KSF-OA samples in deionization water at a concentration of 6.25 × 103 ppm after 15 days is exhibited in Figure 1a. After 15 days, the red emission of the KSF-OA sample still remained. The retention of orange colour of the encapsulated phosphor reveals its excellent moisture resistance. In contrast, no emission is observed for pristine KSF because of the complete hydrolysis of Mn^{4+} to hydrated MnO_2, which precipitates as a brown powder. These results suggest that the KSF-OA phosphor with a hydrophobic, passivating OA skin exhibits good stability in water. By comparably distinguishing, Figure 1b demonstrates the images of pristine KSF, KSF-OA, and KSF-ST phosphors under visible (top layer) and blue light excitation (bottom layer). The enhanced moisture stability was considered by the exceptionally hydrophobic nature of OA and the formation of hydrogen bonds (F···H), as shown in Figure 1c. The KSF phosphor and OA encapsulant exhibit hydrogen bonding (F···H) between the fluorine in KSF and the hydrogen atom of the carboxyl group in OA. OA is an excellent organic hydrophobic material with a high boiling point and the formula $CH_3(CH_2)_7$-CH=CH$(CH_2)_7$COOH, where COOH is the polar headgroup. The remaining long alkyl chain behaves as a strongly hydrophobic tail. The polar KSF molecule, which contains fluorine-terminated moieties, interacts with the polar headgroup (-COOH) of OA through the formation of F···H via hydrogen bonding.

Y. Zhou et al.,[15] used super hydrophobic surface modification with octadecyltrimethoxysilane (ODTMS) on surfaces of a waterproof narrow-band fluoride phosphor $K_2TiF_6:Mn^{4+}$ (KTF) and demonstrated significantly improved moisture-resistance performance, and no obvious changes in thermal stability and the absorption and quantum efficiency. Namely, the luminous efficiency (LE) of the modified KTF was maintained at 83.9% after being dispersed in water for 2 h or aged at high temperature (85 °C) and, moreover, at 84.3% at high humidity (85%) atmosphere (HTHH) for 240 h, respectively, as given in Figures 2a and 2b. Relative emission intensity of modified KTF phosphors was decreasing with a trend that starts steep and later flattens. The decreasing rate has a positive relation with silane; when the carbon chain of silane is longer, the luminescence attenuates more slowly. The WLEDs fabricated with modified KTF phosphor showed excellent colour rendition with lower color temperature (2736 K), higher colour rendering index (CRI, Ra = 87.3, R9 = 80.6), and high luminous efficiency (LE = 100.6 lm/W) at 300 mA.

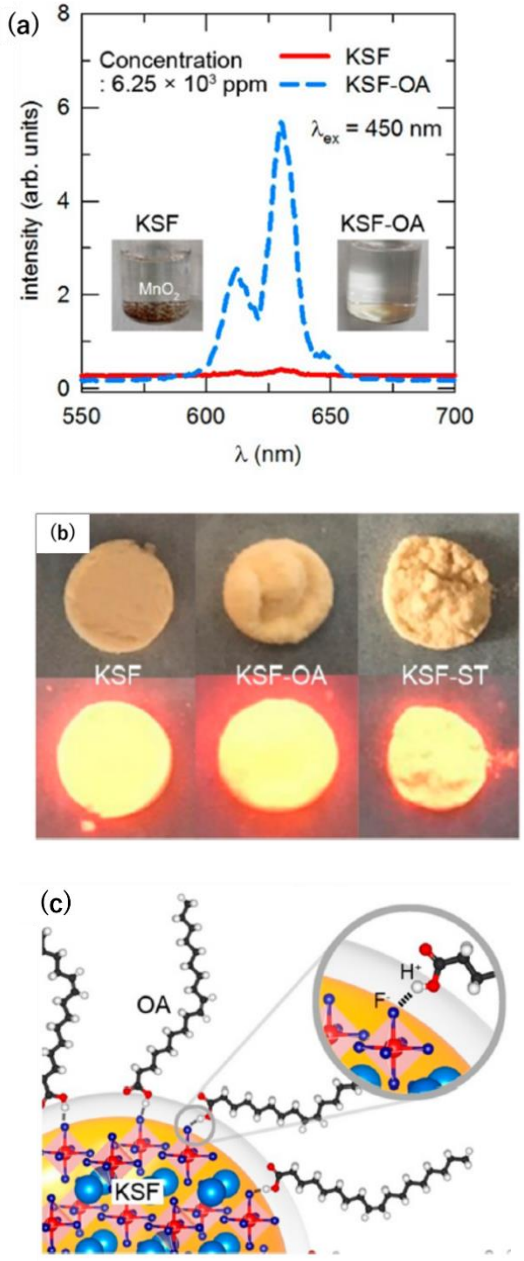

Figure 1. (a) Emission spectra of pristine KSF and KSF-OA samples in deionization water. Inset shows the image of the KSF and KSF-OA samples in the deionized water, (b) Images of pristine KSF, KSF-OA, and KSF-ST (solvothermal) phosphors under visible (top layer) and blue light excitation (bottom layer), and (c) Schematic illustration of the nature of bonding between KSF and OA in the KSF-OA phosphor. The core elements, namely K, Si, and F from the KSF phosphor and shell elements (C, O, and H) of the OA encapsulant are represented as pale blue, red, royal blue, gray, red, and white spheres, respectively.[25]

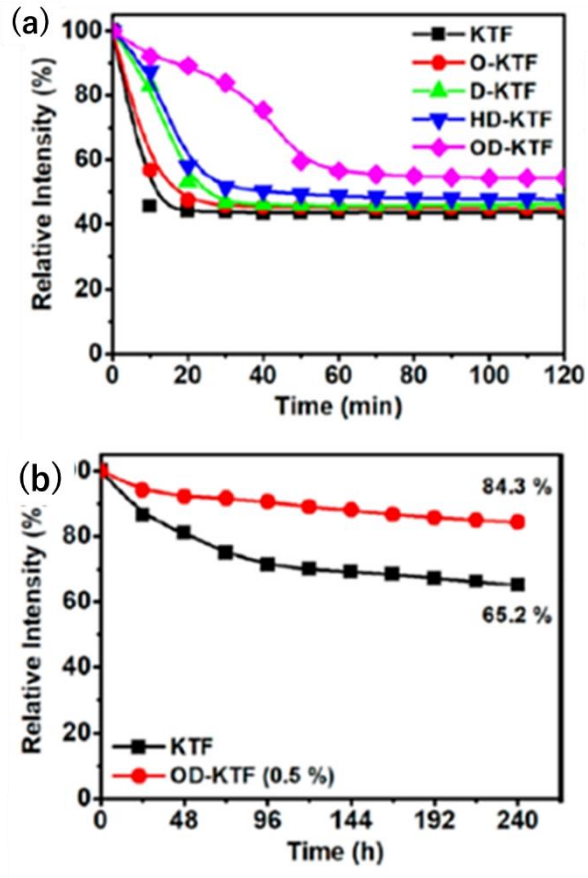

Figure 2. (a) Relative luminous efficiency of KTF and modified KTF (0.5%) in water for 2 h and (b) Relative luminous efficiency of KTF and OD-KTF (0.5%) under an HTHH environment over time for 240 h.[15]

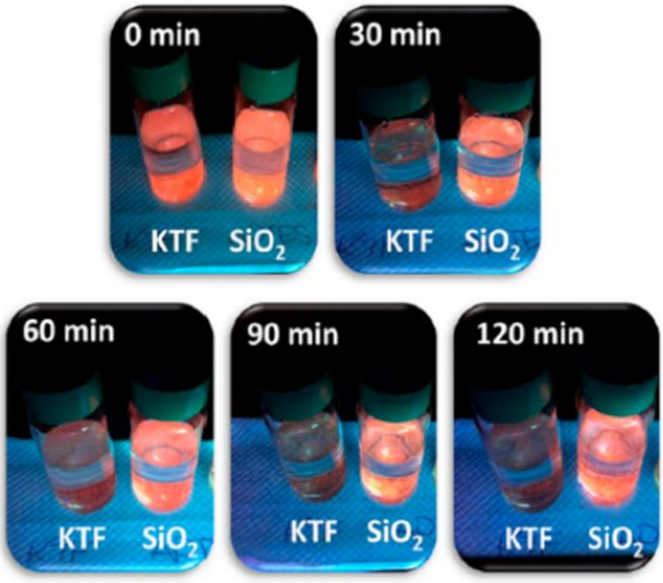

Figure 3. Result of the water resistance test for KTF and KTF@OA@SiO_2 after being placed in an ethanol/water solution at a ratio of 2:3 and excited by 365 nm UV light.[26]

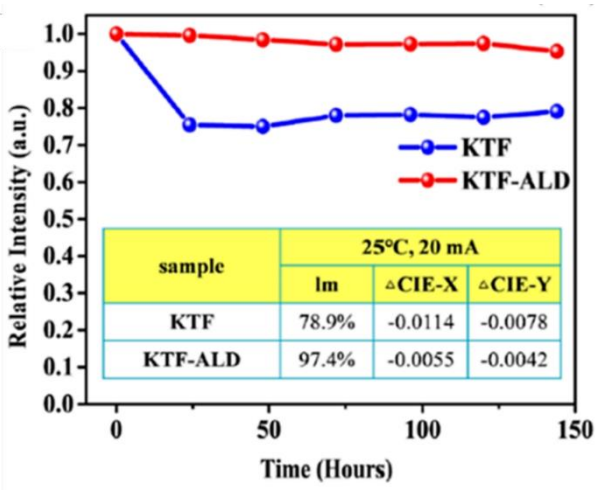

Figure 4. Lifespan of ALD-coated and non-ALD-coated devices.[26]

Fang et al.,[26] proposed integrated surface modification processes to enhance the performance and stability of the luminescence properties of $K_2TiF_6:Mn^{4+}$ (KTF) phosphor. Different concentrations of hydrogen fluoride (HF) solution were used to etch the KTF phosphors; HF could not only reduce the number of small particles and impurities but also increased PL intensity. Moreover, reducing the number of small particles and smoothing the surface of KTF through etching creates a good environment for the subsequent coating process. A double-layer coating consisting of oleic acid (OA) and SiO_2 was used to enhance the chemical stability of the as-prepared powders. Double-shell coating formed a stable protective layer outside the KTF. As-prepared samples were treated with dilute HF solution to remove small particles and impurity, resulting in enhanced PL intensity and improved coating quality. Because of the lack of ligands at the surface of KTF, OA acted as the precursor first, and then triethoxysilane (APTES) and tetraethoxysilane (TEOS) were used to generate a thin SiO_2 layer on the surface. Some of the OA located between the SiO_2 layer and the KTF particle would be dissolved, resulting in a double-layer-coated KTF structure. The luminescent intensity of KTF@OA@SiO_2 particle remains high after 2 h, whereas that of the uncoated particle quickly diminished, as shown in Figure 3. The ALD coating process was used to further protect the surface of the LED device itself from moisture. After exposure to extreme environmental conditions for 144 h, the sample coated via ALD showed a smaller colour point shift compared with the uncoated sample, as given in Figure 4, indicating that the Al_2O_3 layer can effectively diminish colour point shifts. In terms of lifespan of the device, the coated LED demonstrates a better luminescent performance compared with the uncoated LED after a certain period.

Zhou et al.,[16] reported that a facile and general post-synthetic hydrogen peroxide (H_2O_2) surface passivation strategy was proposed to treat the Mn^{4+}-activated red-emitting fluoride phosphors of $K_2XF_6:Mn^{4+}$ (KXF, X = Ti, Si, Ge) in which a Mn^{4+}-rare surface protective layer appeared and further covered the corresponding particles. As shown in Table 1, the environment moisture could be effectively isolated by the Mn^{4+}-rare surface passivation layer with low solubility, which would be sacrificed to protect the phosphor

particles even if under extreme hydrolysis conditions. The relative external quantum efficiency (EQE) of the optimized phosphors still maintains over 96% after the passivation treatment, and the relative luminous intensity still remain 97% even when soaked in water after 12 h. The correlated colour temperature of high-power WLEDs fabricated by the passivated phosphors had no remarkable change during aging process (100 days) in the high temperature (85 °C) and high humidity atmosphere (85%).

Table 1. External quantum efficiency (EQE), relative external quantum efficiency (REQE), internal quantum efficiency (IQE), relative internal quantum efficiency (RIQE), absorption efficiency (AE), and relative absorption efficiency (RAE) of various phosphors before and after treating with H_2O_2 for different times. KTF: $K_2TiF_6:Mn^{4+}$, P-KTF:H_2O-passivated $K_2TiF_6:Mn^{4+}$, KSF: $K_2SiF_6:Mn^{4+}$, P-KSF:H_2O-passivated $K_2TiF_6:Mn^{4+}$, KGF: $K_2GeF_6:Mn^{4+}$, P-KGF: H_2O-passivated $K_2GeF_6:Mn^{4+}$.[16]

Samples	Treating time	EQE(%)	REQE(%)	IQE(%)	RIQE(%)	AE(%)	RAE(%)
KTF	0 min	43.37	100.00	53.80	100.00	80.62	100.00
P-KTF	15 min	52.62	121.32	75.74	140.79	69.47	86.17
	30 min	52.67	121.45	80.08	148.85	66.95	83.04
	45 min	54.74	126.22	81.78	152.01	65.77	81.59
	1 h	51.30	118.29	83.19	154.64	61.67	76.50
	2 h	49.41	113.92	85.44	158.82	57.84	71.74
	4 h	42.58	98.16	83.84	155.84	50.79	63.00
KSF	0 h	30.10	100.00	69.90	100.00	43.00	100.00
P-KSF	24 h	31.50	104.65	78.10	111.73	40.30	93.72
KGF	0 h	59.50	100.00	75.40	100.00	78.90	100.00
P-KGF	24 h	57.60	96.81	75.20	99.73	76.70	97.21

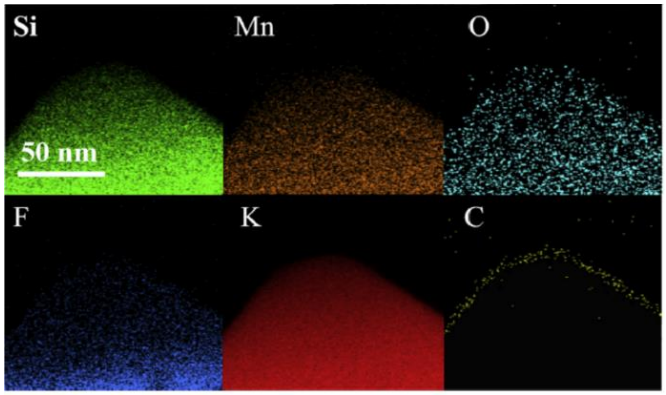

Figure 5. EDS mapping images of KSF@C phosphor.[27]

Liu et al.,[27] reported $K_2SiF_6:Mn^{4+}$ phosphor was coated with an inorganic hydrophobic protective layer of nanoscale carbon layer (~5 nm) (Figure 5) to obtain good moisture resistance by chemical vapor deposition method. They found that most of the deposited carbon was coated on the surface of phosphor crystals in amorphous state, which were bonded with the fluorine element in $K_2SiF_6:Mn^{4+}$ phosphor, forming carbon-fluorine (C–F) covalent bonds, Figure 6a. The moisture resistance of $K_2SiF_6:Mn^{4+}$@C phosphor was improved owing to the protection of the hydrophobic carbon. The relative emission intensity of $K_2SiF_6:Mn^{4+}$@C phosphor could maintain 73% of the initial luminous intensity after immersing in the aqueous solution at room temperature for 8 h, whereas $K_2SiF_6:Mn^{4+}$ phosphor without carbon coating was only 0.7% remaining of the initial value under the same conditions, as shown in Figure 6b.

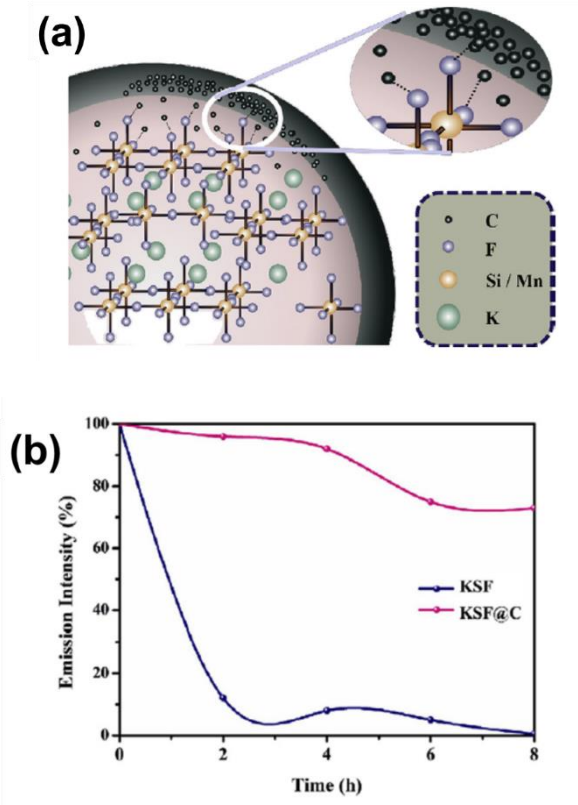

Figure 6. (a) a schematic showing the interaction between the KSF phosphor and the carbon layer in the KSF@C phosphor and (b) emission intensity curves of KSF and KSF@C phosphors after hydrolysis for n hours (n = 0, 2, 4, 6, 8).[27]

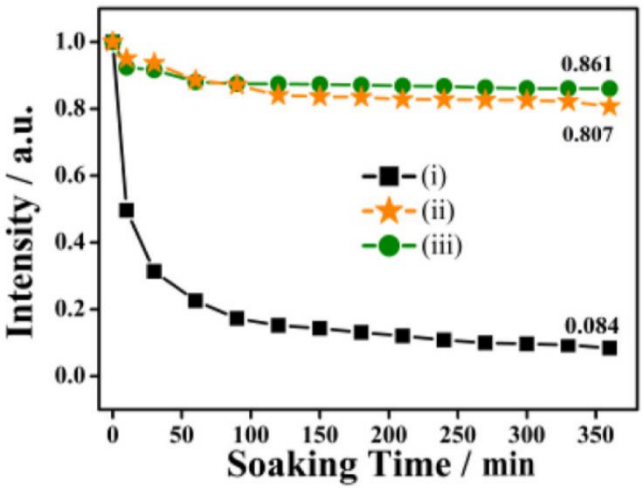

Figure 7. Relative emission intensity changing with different soaking times. i: KSF:Mn^{4+}, ii: P1 (passivation time of 20 min)- KSF:Mn^{4+}, and iii: P2 (passivation time of 30 min)- KSF:Mn^{4+}.[29]

Yu et al.,[28] proposed a method for constructing a homogeneous Mn^{4+}-rare surface shell layer to improve the water-resistant property of $K_2GeF_6:Mn^{4+}$ (KGF) red phosphor by treating with oxalic acid ($H_2C_2O_4$) solution. The moisture-resistant property of the treated KGF (T-KGF) phosphor was significantly enhanced; however, no significant change was observed in its luminescent properties. the Mn^{4+}-rare surface shell layer was in situ deposited on the T-KGF core during the solid-liquid equilibrium process. Upon employing the as-treated TKGF red phosphor, high180-performance white light-emitting diode (WLED) with Ra of 86.3, correlated colour temperature (CCT) of 3824 K, high luminous efficiency (LE) of 152.37 lm/W for WLED2 and an ultrahigh CG (120.1% NTSC standard and 89.7% Rec. 2020 standard) and high LE of 103.12 lm/W for WLED3 were achieved.

A strategy for passivating $K_2SiF_6:Mn^{4+}$ (KSF:Mn^{4+}) phosphor with $Na_2S_2O_4$ was proposed by Deng et al.[29] After passivation, a protective layer was formed on the surface of the phosphor, which significantly enhances the water resistance and fluorescent thermal stability of the optimal sample. The passivated sample could maintain 86.1% of the initial intensity when immersed in water for 6 h, and the fluorescence intensity at 180 °C is 4.11 times of the initial one at 30 °C. The results show that the passivating strategy can improve the NTQ effect of the sample, due to the formation of a protective layer on surface of the sample by passivation, which the layer can prevent energy transfer to surface defects. When the phosphor immersion time lasted up to 6 h, the fluorescence intensity of the sample (i) decreased sharply to 8.4% of the initial value. The fluorescence intensity of the sample (ii) decreased gradually with immersion time but at a much slower rate than the sample (i), where the fluorescence intensity at 360 min (6 h) could be maintained at 80.7% of the initial intensity. The sample (iii) showed a slowly decreasing trend in fluorescence intensity in water compared to the passivated sample, with the remaining 86.1% of the initial fluorescence intensity at 360 min, as shown in Figure 7. The reason for the enhancement of water resistance is that the passivated samples have a rare Mn^{4+} shell layer (KSF) on the surface, which is less soluble in water and prevents hydrolysis of Mn^{4+} in the inner layer.[16, 30–33]

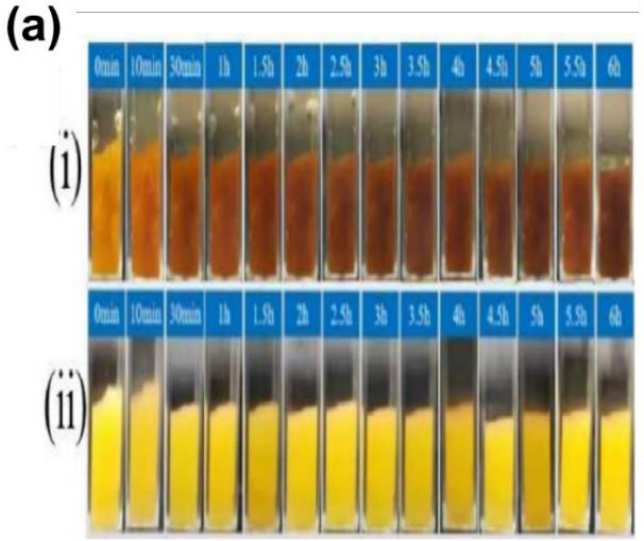

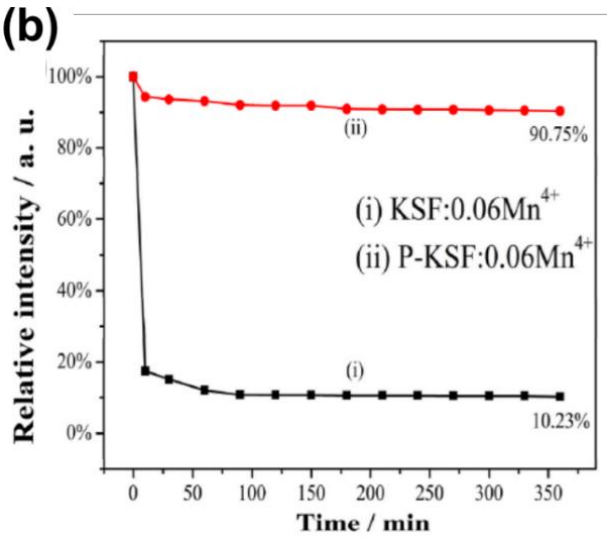

Figure 8. Water resistance test of two samples, (i) KSF:0.06Mn^{4+}, (ii) P (passivation)-KSF:0.06Mn^{4+}: (a) Photographs of phosphor immersed in deionized water, (b) PL integrated intensities with different soaking time in water.[34]

Mn^{4+}-doped fluoride phosphors as red emitting component are used in commercial white light-emitting diodes (WLEDs). However, its application is seriously hindered by its easy hydrolysis. Here, Qiang et al.,[34] proposed to use sodium sulfite as a passivator to treat $K_2SiF_6:Mn^{4+}$. After passivation, a Mn^{4+}-rare K_2SiF_6 protective layer could be formed in situ on the surface of the phosphor, and led to improved emission intensity, luminescent thermal stability and moisture resistance. The formation mechanism of the Mn^{4+}-rare K_2SiF_6 protective layer can be explained by the following equation:[35]

$$K_2Si_{1-x}Mn_xF_6(s) \rightarrow (1-x)[SiF_6]^{2-}(aq) + 2K^+(aq) + x[MnF_6]^{2-}(aq) \quad (1)$$

$$2[MnF_6]^{2-}(aq) + SO_3^{2-}(aq) + HSO_3^-(aq) + 7H^+(aq) + 2H_2O \rightarrow 2Mn^{2+}(aq) + 2SO_4^{2-}(aq) + 12HF(l) \quad (2)$$

$$K_2Si_{1-x}Mn_xF_6(s) + [SiF_6]^{2-}(aq) + 2K^+(aq) \rightleftarrows K_2Si_{1-x}Mn_xF_6@K_2SiF_6(s) \quad (3)$$

First, the surface layer of phosphor in contact with water inevitably dissolves and partially ionizes in solution, forming $[SiF_6]^{2-}$ and $[MnF_6]^{2-}$ anionic groups and K^+, as shown in Eq. (1). Then, the free $[MnF_6]^{2-}$ group reacts with SO_3^{2-} and HSO^{3-} groups and is reduced to Mn^{2+} ion, as shown in Eq. (2). Since the K_2SiF_6 has meagre solubility, the solid-liquid equilibrium is easily reached.[36] Therefore, the $[SiF_6]^{2-}$ group released from Eq. (1) quickly binds to the K^+ to form a K_2SiF_6 protective layer on the phosphor in situ. The process is shown in the reaction Eq. (3). Through the above steps, a Mn^{4+}-rare K_2SiF_6 protective layer is formed in situ on the surface of the sample. When soaking in water for 6 h, the integrated fluorescent intensity of the passivated sample maintained 90.8% of the initial value, while the intensity of the un-passivated sample sharply decreased to 10.2% of the initial value, as exhibited in Figure 8. Mechanisms to improve the emission, water resistance and thermal stability of the luminescence are proposed and discussed. WLED was assembled

with the passivated sample, and good performance of warm white light (CCT = 2963 K, Ra = 90.4) was obtained, as shown in Figure 9.

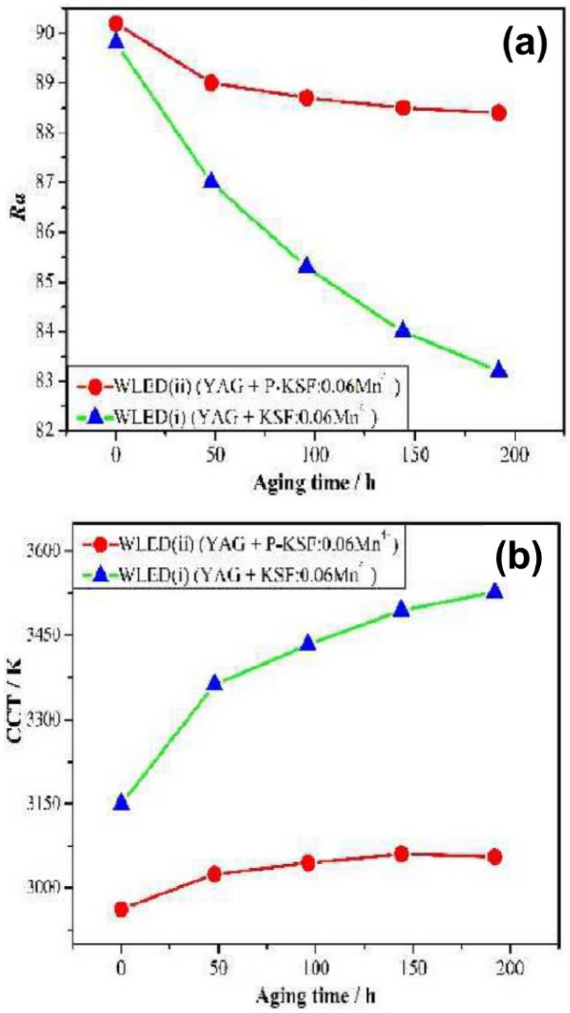

Figure 9. Performances of prototype WLEDs using the mixing phosphors of P-KSF:0.06Mn^{4+} (or KSF:0.06Mn^{4+}) and YAG:Ce^{3+} based on InGaN chip under a 100 mA drive current: (a) color rendering index (Ra) curves and (b) correlated colour temperature (CCT) curves.[34]

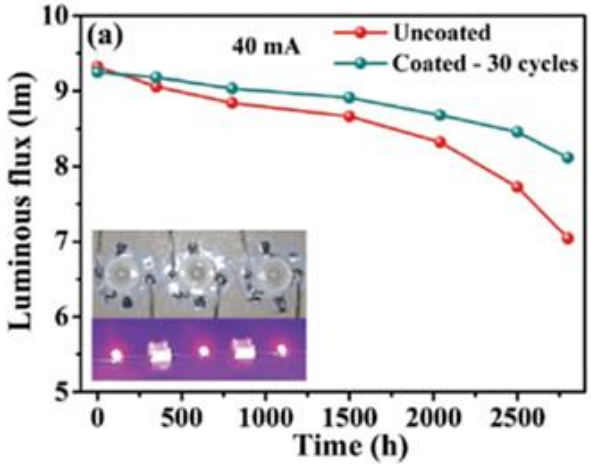

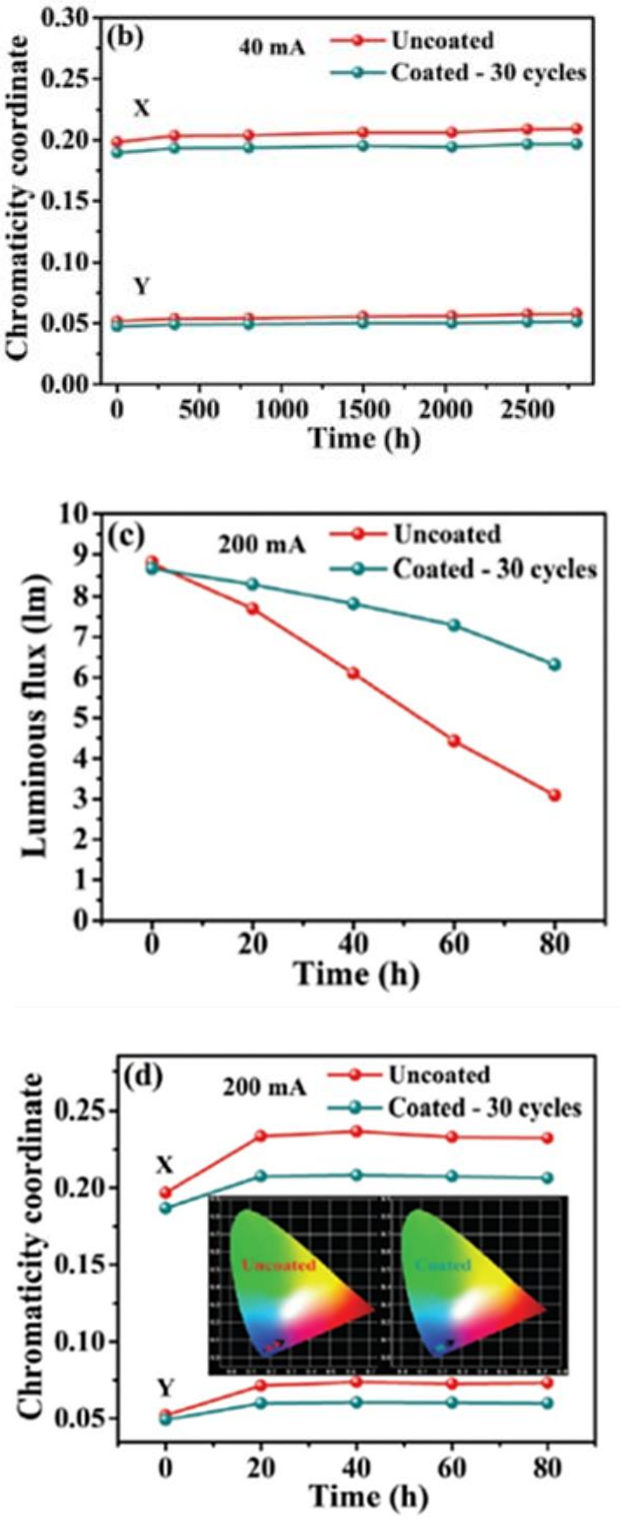

Figure 10. Luminous flux (a and c) and chromaticity coordinates (b and d) of the LEDs fabricated with uncoated KGF and the Al_2O_3 coated KGF with 30 cycles aged under 40 and 200 mA for different times, respectively.[37]

Zhao et al.,[37] utilized the atomic layer deposition (ALD) technique to deposit a passive layer of Al_2O_3 on $K_2GeF_6:Mn^{4+}$ (KGF) phosphor for enhancing its water resistance. The uncoated KGF phosphor was easily decomposed by water, with the $[MnF_6]^{2-}$ group hydrolysed to manganese oxide and the morphology reconstructed.[38, 39] The Al_2O_3 protective layer suppressed the decomposition and hydrolysis of the phosphor and therefore greatly improved its water resistance. The uncoated or the $A_{l2}O_3$ coated KGF powders were combined with commercially available 450 nm LED chips to prepare purple LEDs. The LEDs were driven under 40 mA and 200 mA for different periods, respectively (Figure. 10). As shown, when aged under 40 mA for 2800 h and 200 mA for 80 h, in both cases, the coated KGF phosphor enabled the fabrication of longer lifetime and higher stability LEDs with less aging loss and smaller shifts in chromaticity coordinates. This demonstrates that the Al_2O_3 protective layer produced by ALD allows effective improvement of the reliability of the KGF phosphor and the LEDs.

Sulphide phosphors

Sulphide phosphors are used in white LEDs due to their high emission efficiency, however, unfortunately, sulphide phosphors are prone to degradation when exposed to various environmental factors, such as moisture, oxygen, and temperature changes.[6, 40] Therefore, improving the stability of sulphide phosphor LED coatings is an active area of research, with the goal of developing more durable and efficient LED lighting technologies.

To improve the longevity of a phosphor converted white light-emitting diode (LED), Park et al.,[41] prepared the SiO_2 coating on CaS:Eu phosphor by using polymer binder. The coating characteristics were found to be critically dependent on the sort of monomer and temperature of the reaction during the polymerizing process and meanwhile avoided hydrolysis reaction, Polymer binder coating of SiO_2 on CaS:Eu phosphor was very solid and well served as a protective layer against the moisture.

Avci et al.,[42] reported on the usage of alumina coating for the protection of moisture sensitive $CaS:Eu^{2+}$ micro-particles, with using alumina sol. In situ measurements of accelerated ageing of the luminescent particles, coated particles showed a broad band PL emission with a maximum at 650 nm identical to that of uncoated particles and coating with an alumina layer drastically increased the resistivity of the luminescent material against moisture.

Yoo et al.,[43] improved the stability of $CaS:Eu^{2+}$ phosphors with respect to moisture, surface coating with poly(methylmethacrylate) $(PMMA)^{+}$–silica nanocomposites. Formation of a PMMA–silica nanocomposite on the surface of the phosphor after coatings was confirmed and an increase in the PL intensity was observed after coating, determined by the coating method. The moisture resistance of the phosphors before and after coating was examined by aging in a temperature-controlled humidity chamber at 100 °C and 80% relative humidity. A decreasing intensity for the uncoated phosphor, in contrast to a nearly constant value for coated phosphors with aging time, was observed in Figure 11. The PL intensity was reduced by about 55% after 7days. These results indicate that $CaS:Eu^{2+}$ phosphor is very unstable when it is exposed to moisture, in contrast to a decreasing intensity for the uncoated phosphor, indicating that the PMMA–silica nanocomposite coating on the phosphors served as a protective layer by retarding the surface-related damage caused by moisture.

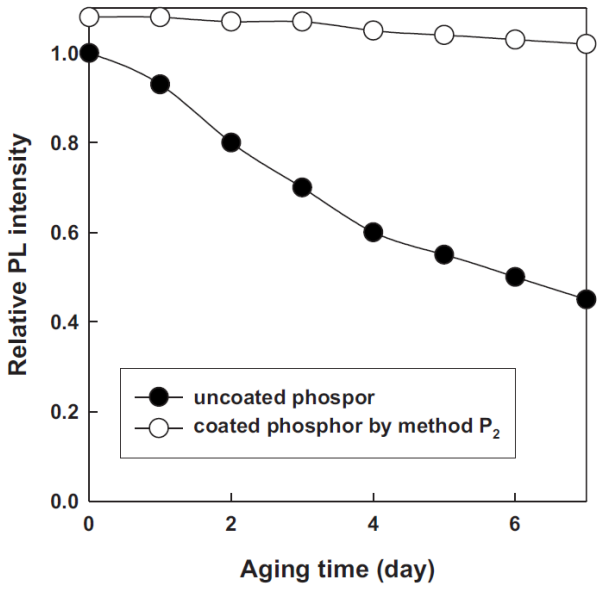

Figure 11. Normalized PL intensity as a function of the cumulated aging time for uncoated and coated phosphors. Phosphors were aged in a temperature-controlled humidity chamber at 100°C and 80% RH.[43]

Silicate phosphors

Alkaline earth silicate phosphors can emit various colourful lights, depending on the doping rare earth elements, making them a popular choice for many lighting and display applications. In recent years, there have been significant researches on developing new types of silicate phosphors with improved properties, such as higher brightness, and better stability for further enhancing the performance of lighting and display devices and contributing to the development of more efficient and sustainable technologies.[44–46] Instead of this, forming a protective coating layer around surface of phosphor particles becomes an easy and efficient method for achieving property strengthen.

In order to improve the phosphor efficiency of yellow emission of the phosphor-converted white light emitting diode (pcW-LED), Lee et al.,[47] reported that the Ba^{2+} Mg^{2+} co-doped Sr_2SiO_4:Eu phosphors were synthesized and were coated with thin and uniform TiO_2 with 20 nm thickness. The PL properties of the TiO_2-coated phosphors showed improved yellow-emission intensity compared to the pristine phosphors. The TiO_2 coating yielded an improvement (9%) in the phosphor efficiency because the thin TiO_2 layer was formed uniformly over the phosphor surface, as shown in Figure 12a. The absorbance spectra for the pristine phosphor and the TiO_2-coated phosphors were measured by the UV–vis/DR spectra shown in Figure 12b. After coating, however, the photons mainly transmit the TiO_2 layer via increase absorption in the range of 400–500 nm due to low refractive index of the amorphous TiO_2 and then get to the phosphor surface compared to pristine phosphor. Therefore, the effective excitation absorption of the phosphor via the TiO_2 layer occurred.

The temperature dependence of PL was measured from 25 to 150 °C. The TiO_2-coated phosphors showed superior thermal quenching property compared to pristine phosphors, as exhibited in Figure 13. With increasing temperature up to 150 °C, the relative PL intensity of TiO_2-coated phosphors was decreased to 78% of the initial value, whereas it was 60% for the pristine phosphors. A little bit decrease of PL intensity for pristine phosphors and TiO_2-coated phosphors at room temperature after 120 min was observed about 98% of the initial values and both phosphors show similar PL intensities. But, at 150 °C, the TiO_2-coated phosphors have a better PL intensity than pristine phosphors because TiO_2-coated phosphors showed high thermal quenching stability. These results imply that the pristine phosphor with orthosilicate structure becomes soft at high temperature above 100 °C due to increasing Si–O distance, so that the electrons in the soft structure easily vibrate.[41] From this result, orthosilicate phosphor was confirmed the strong temperature quenching at temperature above 100 °C. However, the TiO_2-coated phosphors showed higher thermal quenching stability. This is expected that the TiO_2 coatings were to inhibit thermal degradation of orthosilicate phosphors due to their chemical, thermal stability and wide band-gap.[48]

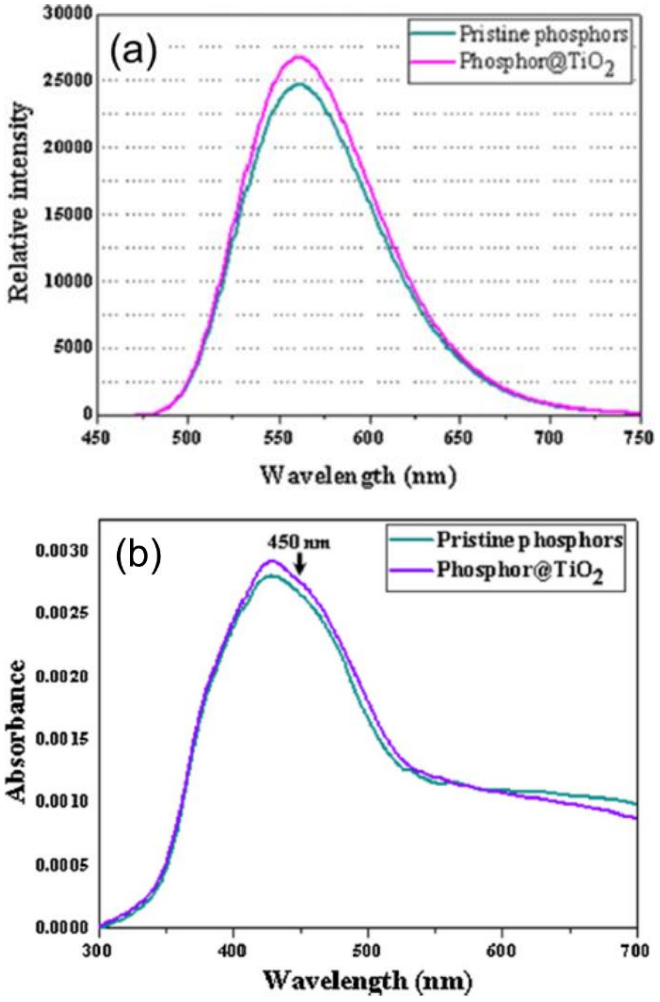

Figure 12. (a) The emission spectra of pristine phosphors and phosphor@TiO_2 and (b) the absorbance of pristine phosphor and phosphor@TiO_2 measured.[47]

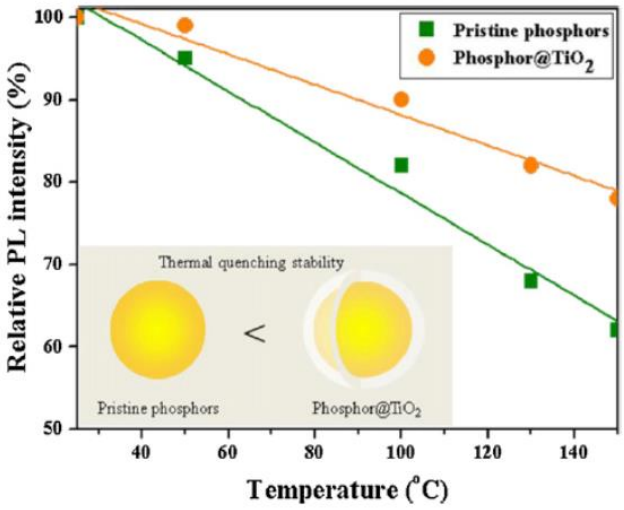

Figure. 13 The temperature dependences of the relative PL of pristine phosphor and phosphor@TiO_2. Inset: proposed schematic diagram showing the thermal quenching stability of phosphor@TiO_2 [47].

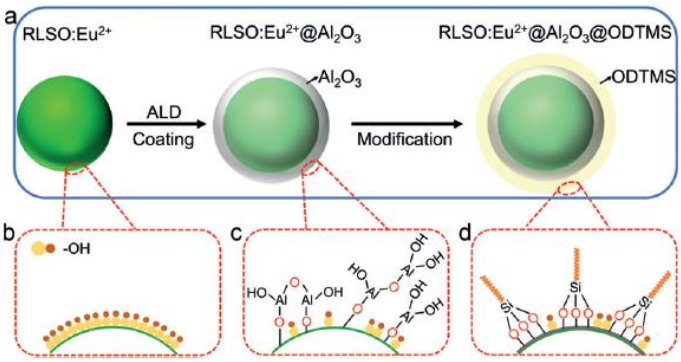

Figure 14. (a) Schematic illustration of surface coating via atomic layer deposition (ALD) for the RLSO:Eu^{2+} phosphor and subsequent hydrophobic surface modification with ODTMS on RLSO:Eu^{2+}@Al_2O_3 surface, Schematic illustrations of (b) the RLSO:Eu^{2+} phosphor surface, (c) the possible ligand formation mechanism of alumina on the phosphor surface during the ALD process, and (d) the nature of the bonding between RLSO:Eu^{2+}@Al_2O_3 and ODTMS.[49]

Poor chemical stability of narrow-band green-emitting $RbLi(Li_3SiO_4)_2:Eu^{2+}$ (RLSO:Eu^{2+}) phosphor hinders their further commercialization in LEDs, even if they have excellent stability against thermal quenching. An efficient protection scheme was proposed by M. Zhao et al.,[49] that the surface coating of amorphous Al_2O_3 and hydrophobic modification were combined by octadecyltrimethoxysilane (ODTMS) to construct the moisture-resistant dual-shelled RLSO:Eu^{2+}@Al_2O_3@ODTMS composite, as schematically illustrated in Figure 14. As a result, good moisture stability with maintain 76% of its initial emission intensity after being immersed in water for 1h was obtained after the surface coating (Figure 15). The stability of RLSO:Eu^{2+}@Al_2O_3@ODTMS after the dual layered protection method treatment exhibits significant improvement towards water erosion. The Al_2O_3 coating layer

fabricated via ALD is dense regardless of the irregularly shape of RLSO:Eu^{2+} particles.[5] It increases the intrinsic protection of water permeation.[50, 51] Meanwhile, the Al_2O_3 coating layer provides a uniform surface with -OH groups for further ODTMS coating, thus a continuous and hydrophobic organic layer is formed. Hence, the composite protective layer can remarkably improve the moisture-resistant property of RLSO:Eu^{2+} phosphors. This shows remarkably improved the water-stability of this narrow-band green emitter and as a promising candidate for the high-performance display backlights.

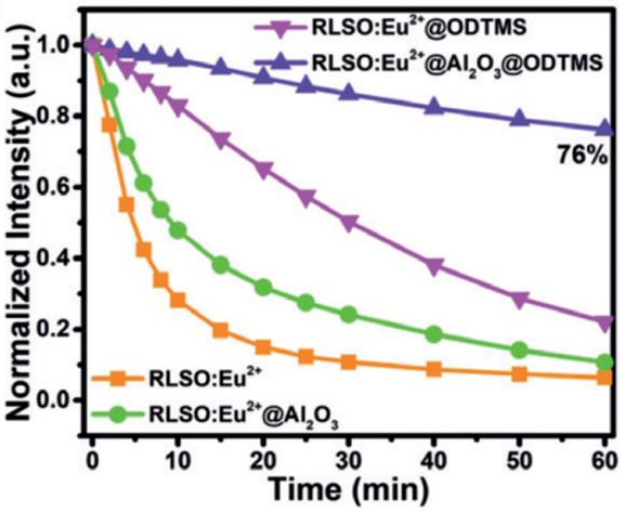

Figure 15. Time-dependent normalized PL intensities of RLSO:Eu^{2+}, RLSO:Eu^{2+}@Al_2O_3, RLSO:Eu^{2+}@ODTMS, and RLSO:Eu^{2+}@Al_2O_3@ ODTMS immersed in water.[49]

Oxide phosphors

Even though most oxide-based phosphors have low absorption in the visible-light spectrum, making it impossible for them to be coupled with blue LEDs, some rare-earth oxide phosphors are well-known red down-conversion phosphors used in commercial lighting and display technology, as well as recently in organic light emitting diodes (OLEDs). In particular, nanoscale Eu:Y_2O_3 can shift and broaden the absorption band, which can improve the direct excitation by UV-LEDs, but unfortunately the nanocrystals still lack a large spectral cross section in the appropriate spectral range for efficient pumping of the phosphor by a UV-LED. Therefore, the use of a passivating ligand on a nanocrystal as a molecular antenna for enhancing the optical cross section for absorption of the exciting LED energy.

Eu(III)-doped Y_2O_3 nanocrystals were prepared by microwave synthetic methods as spherical 6.4±1.5 nm nanocrystals with a cubic crystal structure and the surface of the nanocrystal was passivated by acetylacetonate (acac) and 1-hexadecylamine (HAD) on the Y exposed facet of the nanocrystal, reported by Dai et al.[52] Excitation into the $S_0 \rightarrow S_1$ ($\pi \rightarrow \pi^*$) or acac$\rightarrow Ln^{3+}$ LMCT transition led to the production of white light emission arising from efficient intramolecular energy transfer to the Y_2O_3 oxygen vacancies and the Eu(III) Judd–Ofelt f–f transitions. The acac passivant was thermally stable below 400 °C and the presence of the low-lying acac levels allowed UV LED pumping of the solid phosphor, leading to high quantum efficiency (~19%) when pumped at 370 nm, high-quality white light colour rendering (CIE coordinates 0.33 and 0.35), a high scotopic-to-photopic ratio (S/P = 2.21), and thermal stability. In a LED lighting package luminosity of 100 lm/W were obtained, which are competitive with current commercial lighting technology. The use of the passivation to funnel energy to the lanthanide emitter via a molecular antenna effect represents a new paradigm for designing phosphors for LED-pumped white light.

Nitride phosphors

$Sr_2Si_5N_8$:Eu^{2+} is one of the well-known red phosphors as a promising red colour component applied in white LEDs.[2] In the orthorhombic crystal structure of the $Sr_2Si_5N_8$ host (space group Pmn21), Eu^{2+} ions, activators, occupy the Sr sites in the lattice due to their similar ionic radii. The SiN_4 tetrahedra build up a three-dimensional network by corner-sharing N atoms to form a rigid framework, rendering the phosphor highly chemically and thermally stable.[53] Besides, when excited at the 450 nm wavelength, the $Sr_2Si_5N_8$:Eu^{2+} phosphor gives strong emission in the red region of 616–670 nm with high quantum efficiency.[54, 55] However, one of the main problems encountered in the red phosphor of $Sr_2Si_5N_8$:Eu^{2+} is serious thermal degradation of PL properties, leading to low reliability and a shorter lifetime of white LED devices.[56] In this case, how to reduce the influence of thermal degradation on the luminescence property of the $Sr_2Si_5N_8$:Eu^{2+} phosphor becomes more significant for the application in white LEDs.

Passivation, referring to a material becoming ''passive'', makes a shielding outer-layer of the base material. Currently, surface passivation as a promising technique has been not only limited in protecting metals or alloys against corrosion, more importantly, but also has been extended to improve the performance of materials, extensively in reducing surface recombination in solar cells.[57–59]

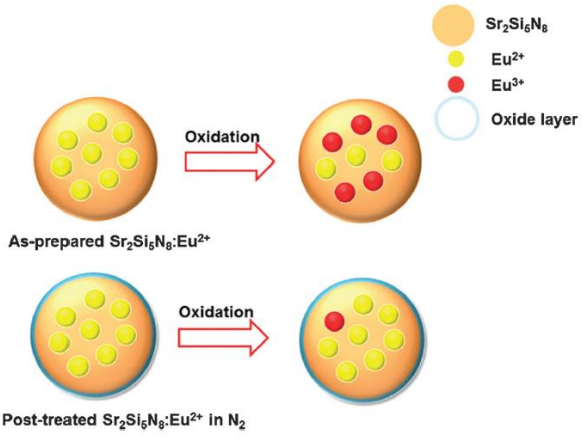

Figure 16. Schematic illustration of the contribution of oxide compound layer formed around the $Sr_2Si_5N_8$:Eu^{2+} surface via thermal treatment in N_2 in preventing activator Eu^{2+} ions from being oxidized.[60]

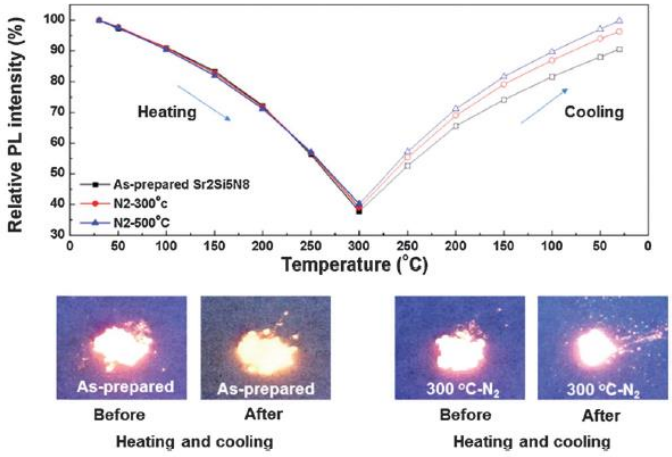

Figure 17. Relative PL intensities of the as-prepared and N_2-treated $Sr_2Si_5N_8:Eu^{2+}$ phosphors with heating (heating from 30 °C to 300 °C) and cooling (from 300 °C to 30 °C) to indicate the influence of thermal degradation on PL intensity. The insets are the photographs of the as-prepared and 300 °C-N_2 treated phosphor powders excited in a 365 nm-UV box before and after heating and cooling processes when determining thermal degradation properties.[60]

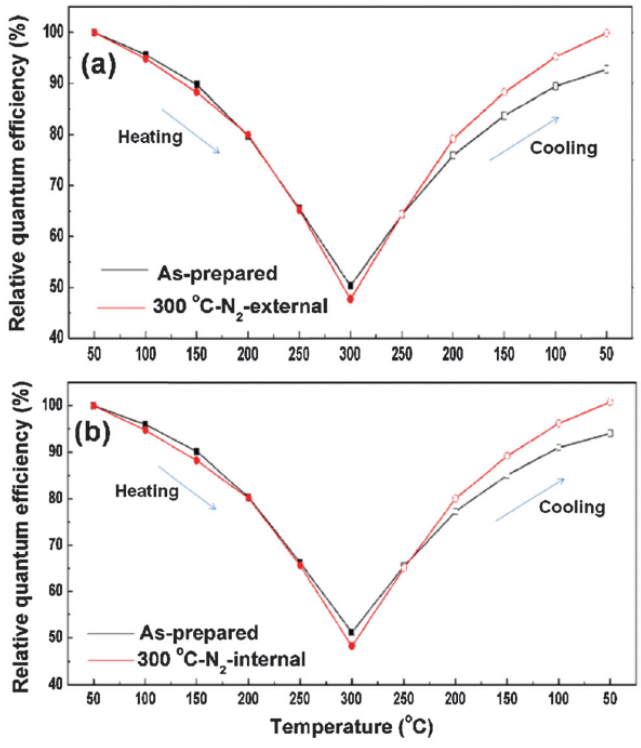

Figure 18. Temperature-dependent external and internal QEs of the as-prepared and 300 °C-N_2 treated $Sr_2Si_5N_8:Eu^{2+}$ phosphors with heating (from 50 °C to 300 °C) and cooling (from 300 °C to 50 °C) temperatures to indicate the influence of thermal degradation on PL intensity.[60]

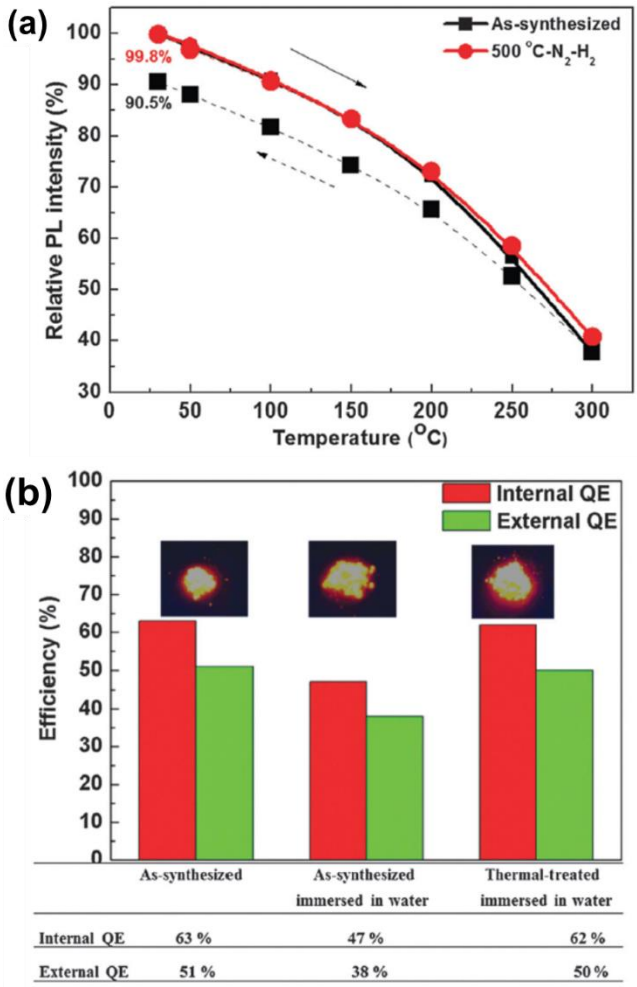

Figure 19. (a) Temperature-dependent relative PL intensities of the as-synthesized and 500 °C-treated $Sr_2Si_5N_8:Eu^{2+}$ phosphors in N_2–H_2 upon heating up to 300 °C and then cooling down to 30 °C and (b) Internal and external QEs of the as-synthesized and thermally-treated $Sr_2Si_5N_8:Eu^{2+}$ powders after being immersed in water at 200 °C for 1 h by comparing with those of the as-synthesized phosphor before the water immersion. Inset images of these phosphor powders irradiated at 365 nm by a handy UV lamp.[61]

The as-synthesized red phosphor of $Sr_2Si_5N_8:Eu^{2+}$ were post-treated in a N_2 atmosphere by Zhang et al.[60] After the thermal treatment in N_2, it was found that the N_2-treatment caused a negligible influence on the phase purity and particle morphology. The surface of the phosphor particle became more hydrophilic. The edge area (formed surface layer) of the phosphor particle had lower CL intensity than the inner part but it inhibited the surface damage caused by e-beam irradiation and the formed surface layer plays a passivating role in preventing the Eu^{2+} activator from being oxidized, consequently, effectively reducing thermal degradation that deteriorates the PL intensity of the $Sr_2Si_5N_8:Eu^{2+}$ phosphor, due to the formation of the passivating layer around the phosphor particle against the activator Eu^{2+} being oxidized, as illustrated in Figure 16. As shown in Figure 17, the recovered relative PL intensity of the phosphor after heating up to 300 °C and then cooling down to 30 °C

was 90.5% of the initial intensity. In comparison, the recovered relative PL intensity of the N_2-treated phosphor was significantly improved: 96.3% of the initial intensity under 300 °C-treatment and 99.8% under 500 °C-treatment, indicating that the thermal-treatment in N_2 as a post-treatment way reduced the influence of the thermal degradation on PL intensity. Furthermore, the contribution of the thermal-treatment in N_2 on decreasing the thermal degradation on PL intensity can also be more accurately found in the temperature-dependent external and internal QEs of the as-prepared and 300 °C-N_2 treated $Sr_2Si_5N_8$:Eu^{2+} phosphors with heating (from 50 °C to 300 °C) and cooling (from 300 °C to 50 °C) temperature (Figure 18). When temperature cooling down to 50 °C, the recovered external and internal QEs of the 300 °C-N_2 treated phosphor were 99.5% and 99.8% appreciably higher than those of 92.7% and 94.1% of the as-prepared $Sr_2Si_5N_8$:Eu^{2+}, respectively.

Figure 16. Schematic illustration of the contribution of oxide compound layer formed around the $Sr_2Si_5N_8$:Eu^{2+} surface via thermal treatment in N_2 in preventing activator Eu^{2+} ions from being oxidized.[60]

The synthesized red phosphor of $Sr_2Si_5N_8$:Eu^{2+} was thermally post-treated in an inert and reductive N_2–H_2 mixed-gas atmosphere at 300–1200 °C by Zhang et al.[61] A passivation layer of ~0.2 mm thickness was formed around the phosphor surface via thermal treatment. Thermal and moisture-induced degradation of PL intensity was effectively reduced by the formation of a passivation layer around the phosphor surface, that is, the relative PL intensity recovered 99.8% of the initial intensity even after encountering thermal degradation; both moisture-induced degraded external and internal QEs were merely 1% of the initial QEs, as shown in Figures 19a and 19b, respectively. The formed surface layer was concluded to primarily prevent the Eu^{2+} activator from being oxidized, based on the systemic analysis of the mechanisms of thermal- and moisture-induced degradation. That is, the origin of the thermal degradation in $Sr_2Si_5N_8$:Eu^{2+} was proposed to the oxidation of Eu^{2+}.[62] From the crystal structure of the $Sr_2Si_5N_8$:Eu^{2+}, it has been known that the Eu^{2+} activator in the layer-structured host lattice of $Sr_2Si_5N_8$ is inserted between the [SiN_4] tetrahedral layers,[53] therefore enabling the charges to readily transfer from dopant ions to oxygen ions when Eu^{2+} activators are close to O_2.[63] The oxidation process is expressed by the following equation:

$$2\mathrm{Eu}^{2+} + \frac{1}{2}\mathrm{O}_2(\mathrm{g}) + \mathrm{V}_{\ddot{\mathrm{O}}} \rightarrow 2\mathrm{Eu}^{3+} + \mathrm{O}_{\mathrm{O}}^{\times} \qquad (4)$$

where Eu^{2+} is the divalent europium ion, $O_2(g)$ is the gaseous oxygen atom, $O_O^{\times}$ is the oxygen vacancy, Eu^{3+} is the trivalent europium ion, and $V_{\ddot{O}}$ is the oxygen ion of the lattice, "·" and "×" are the Kröger-Vink notations for the net charge +1 and the zero net charge, respectively. However, the mechanism of the degradation of PL property induced by the moisture attacks differs from that induced by thermal attack. An oxidant gas penetration mechanism was proposed to explain why oxidation reaction is more active in moist air than in dry air.[64] It is proposed that the hot water may lead to consume the nitrogen component in the $Sr_2Si_5N_8$ host and made the host lattice being oxidized by catching O from H_2O. Such oxidation first occurred at the phosphor particle surface and then preceded into the inner part of the particle via penetration through the cracks existing at the particle surface under the moisture atmosphere. In this case, the contribution of the passivation layer is considered to play a role in protecting the Eu^{2+} ions from heat and humidity, making the $Sr_2Si_5N_8$:Eu^{2+} red phosphor more suitable for use in white LEDs.

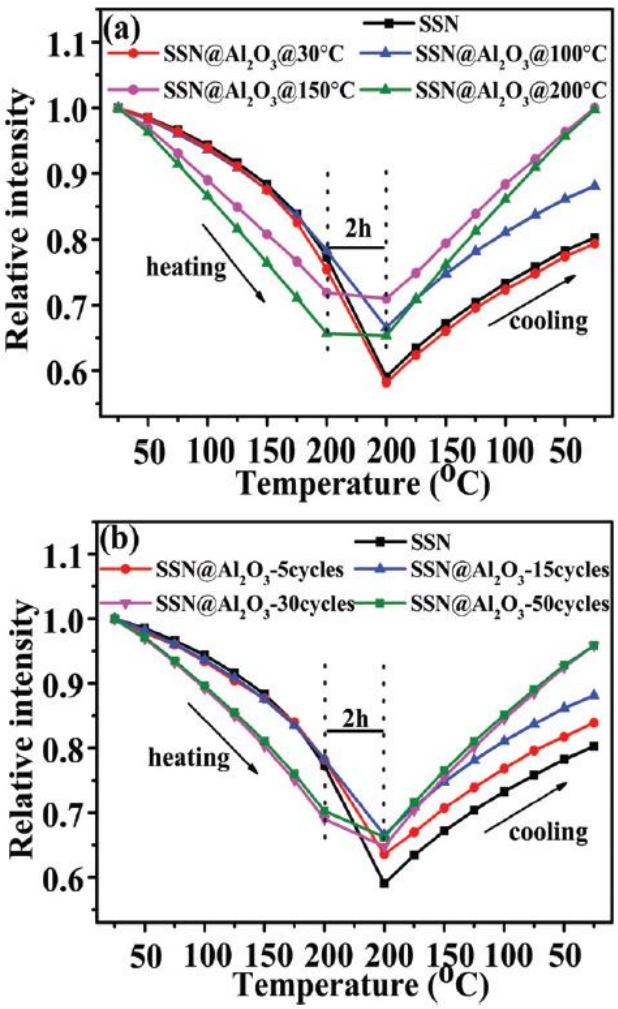

Figure 20. Temperature-dependent PL in air of SSN and SSN@Al_2O_3 (a) coated at different temperatures and (b) coated at 100 1C with different numbers of cycles.[65]

The red-emitting $Sr_2Si_5N_8$:Eu^{2+} (SSN) phosphor with a superior quantum efficiency and suitable emission spectrum has been widely used as a promising down-conversion material in white light-emitting diodes. However, its thermal degradation under high temperature handicaps its large-scale application. Here, Zhao et al.,[65] proposed to increase the thermal stability of $Sr_2Si_5N_8$:Eu^{2+} by coating a nanometre-order Al_2O_3 film on each phosphor particle using an atomic layer deposition approach in a fluidized bed reactor. The deposited Al_2O_3 layer was quite uniform and conformal when using O_3 as the oxidizer, and its thickness could be controlled by the dosage type, deposition temperature and cycle numbers, which largely affects the PL properties and thermal degradation of the title phosphor. The optimum deposition temperature of Al_2O_3 was in the range of 100–150 °C, and the number of deposition cycles was in the range of 15–30 cycles at 100 °C. Thermal gravimetric analysis results showed that the oxidation temperature of the coated phosphor

increased from 700 to 850 °C, suggesting that the coating layer has the function of anti-oxidation. Consequently, the thermal degradation of phosphor powders in air at 200 °C was greatly reduced, owing to prevention from oxidizing host lattice by the coating layer, as shown in Figure 20. The uncoated SSN could recover 80% of the original luminescence intensity after a heating–cooling cycle, and the sample coated at 30 °C recovers about 79%. It also means the serious thermal degradation of these samples. When the deposition temperature increases, the thermal degradation of the coated samples decrease and it totally disappears for the samples coated at 150 and 200 °C. The enhanced thermal stability with increasing deposition temperature could be ascribed to the following reasons. (i) A higher deposition temperature results in less water incorporated in the Al_2O_3 layer, (ii) the hydrophobic surface restrains the water-assisted degradation, and (iii) a higher deposition temperature already causes degradation of the phosphor during coating. With increasing number of coating cycles (i.e., film thickness) at 100 °C, the thermal degradation could also be reduced and 95% of the luminescence is recovered. In addition to the thicker Al_2O_3 coating layer which can provide better protection of SSN against oxidation, the hydrophobic surface also has the role of protection.

Oxynitride phosphors

The surface defects in the oxynitride (sialon) phosphor particles are considered as an important factor, impairing its PL efficiency because of the luminescence quenching by the defects. These surface defects are generally formed by the surface damage from the post-treatment such as pulverization after the synthesis reaction, since the phosphor prepared by the solid-state reaction is usually agglomerated and thus needs to be controlled by the post-treatment.[12] Therefore, if these defects could be repaired by the surface modification of the phosphor particles, PL efficiency of the phosphor would be improved and therefore be more suitably for application in power-saving and high-efficiency LED.[47, 66, 67] It has been reported that some surface groups, generally involving acidic (Si-OH) and basic (Si_2-NH) groups, inhabit at the silica-rich surface of silicon nitride particle, of which silanol (Si-OH) groups mainly act as surface active sites on the particle surfaces. By utilizing these surface groups in oxynitride phosphors.[68, 69] Zhang et al.,[70] reported that Ca-α-SiAlON: Eu^{2+} phosphor powder was modified with a SiO_2 coating by the adsorption, hydrolysis, and polymerization of the TEOS precursor. The oxidized surface layer of Ca-α-SiAlON exists in the surface groups of Si-OH and Si_2-NH. In this work the existing Si-OH surface group reacted with the added TEOS to create Si-O-$Si(OR)_3$ and then covered the surface of the Ca-α-SiAlON:Eu^{2+} particle by chemical adsorption. Upon the H_2O addition, the hydrolysis reactions then took place linking the alkoxide molecules by a polymerization type of sol–gel reaction. All the reactions in this experiment are described as given below:

Chemical adsorption:

$$\equiv Si–OH+RO–Si(OR)_3 \rightarrow \equiv Si–O–Si(OR)_3 +ROH \quad (5)$$

Hydrolysis and polymerization:

$$\equiv Si–O–Si(OR)_3 +RO–Si(OR)_3+H_2O\rightarrow \equiv Si–O–Si(OR)_3 +HO–Si(OR)_3+ROH \quad (6)$$

$$\equiv Si–OH+RO–Si(OR)_3\rightarrow \equiv Si–O–Si(OR)_3+ROH \quad (7)$$

Through the modification for the surface defects of the particles by the SiO_2 coating, the PL emission could be significantly strengthened in the SiO_2-coated Ca-α-SiAlON: Eu^{2+} powder, as shown in Figure 21.

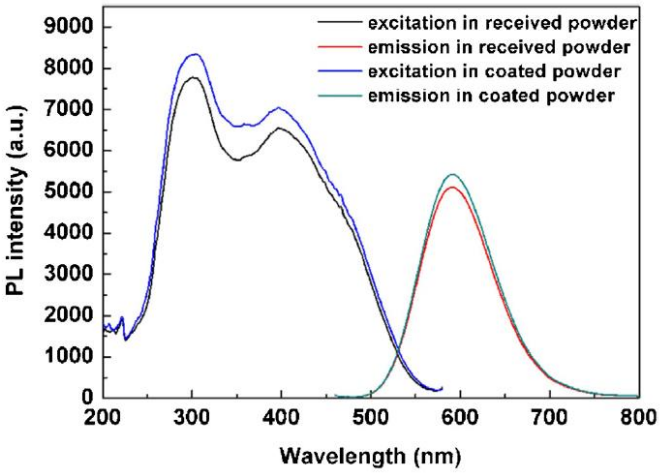

Figure 21. Excitation and emission spectra of the as-received and SiO_2-coated Ca-α-SiAlON: Eu^{2+} powders. λ_{exc}=450 nm for the emission and λ_{em}=590 nm for the excitation.[70]

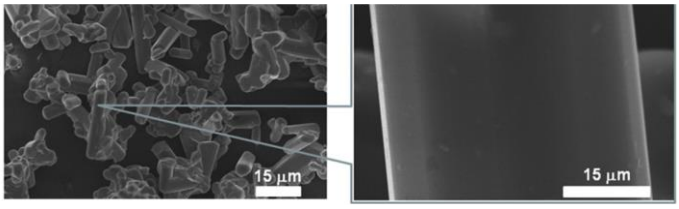

Figure 22. SiO_2-coated β-sialon:Eu^{2+} powders prepared at molar ratio of TEOS:H_2O=1:1 and enlarged local images for the single phosphor particle.[71]

The surface modification on the β-sialon:Eu^{2+} phosphor particles was successfully achieved by the SiO_2 coating via a sol-gel method, reported by Zhang et al.,[71] as demonstrated in Figure 22.The PL intensity of the phosphor was effectively enhanced and dominantly depending on the homogeneity of the SiO_2 coating. It was found that more homogeneous and smoother SiO_2 coating was responsible for higher PL intensity. The strongest emission intensity was obtained after the SiO_2 homogenously coating under an optimized preparation condition by improving ~39% of intensity compared to that of the uncoated β-sialon:Eu^{2+} phosphor, due to effective elimination on the surface groups of the phosphor particles, as shown in Figure 23.

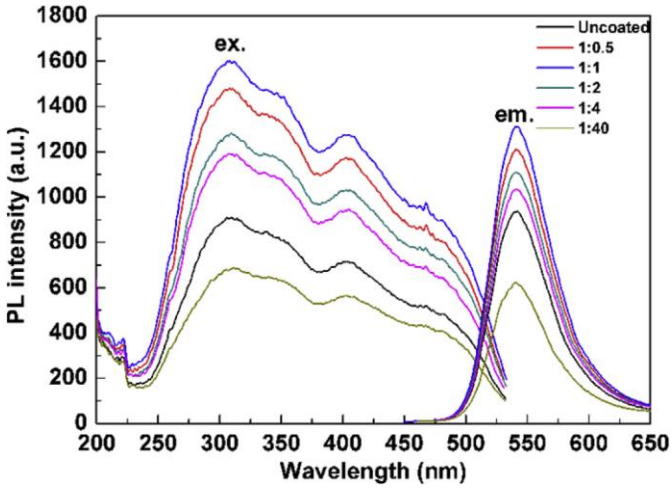

Figure 23. PL spectra of the as-received and SiO_2-coated β-sialon:Eu^{2+} powders prepared at various molar ratios of TEOS:H_2O from 1:0.5 to 1:40. The excitation spectra were monitored at 541 nm and emission spectra were excited under 405 nm.[71]

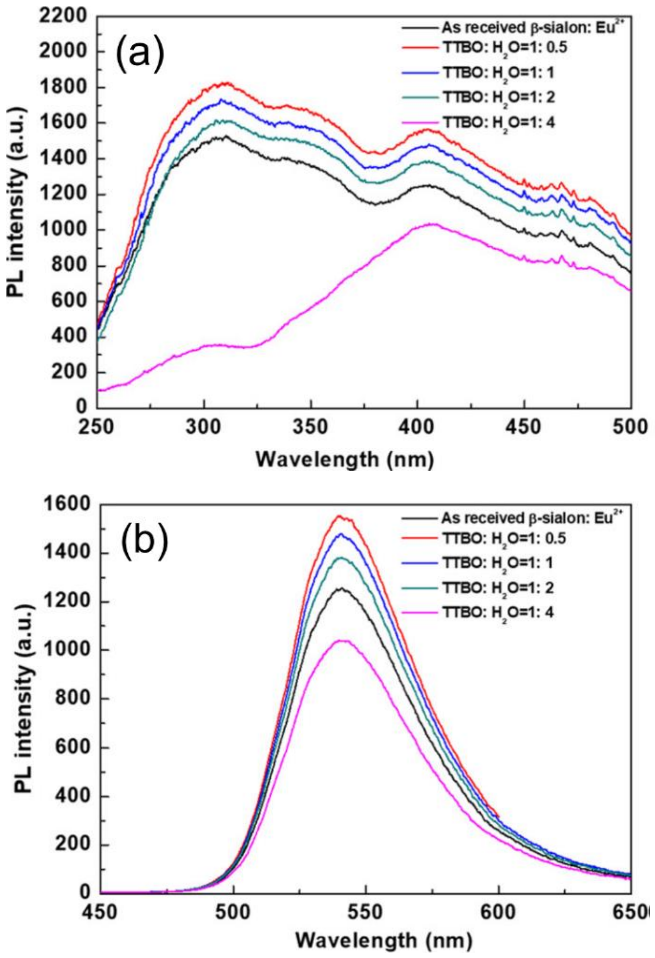

Figure 24. (a) Excitation spectra monitored at 541 nm and (b) Emission spectra under 365 nm excitation of the β-sialon:Eu^{2+} and TiO_2-coated β-sialon:Eu^{2+} (prepared at TTBO:H_2O = 1:0.5, 1:1, 1:2, and 1:4 in volume ratios).[72]

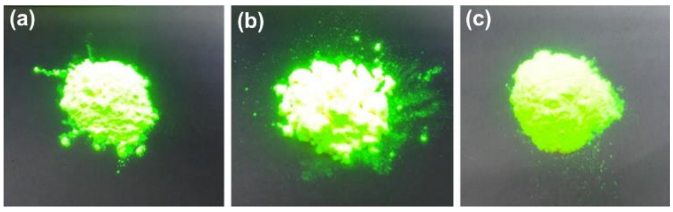

Figure 25. Brightness comparison under the 365 nm irradiation for the (a) β-sialon:Eu^{2+} and TiO_2-coated β-sialon:Eu^{2+} prepared at (b) TTBO:H_2O = 1:0.5 and (c)1:4 in volume ratios.[72]

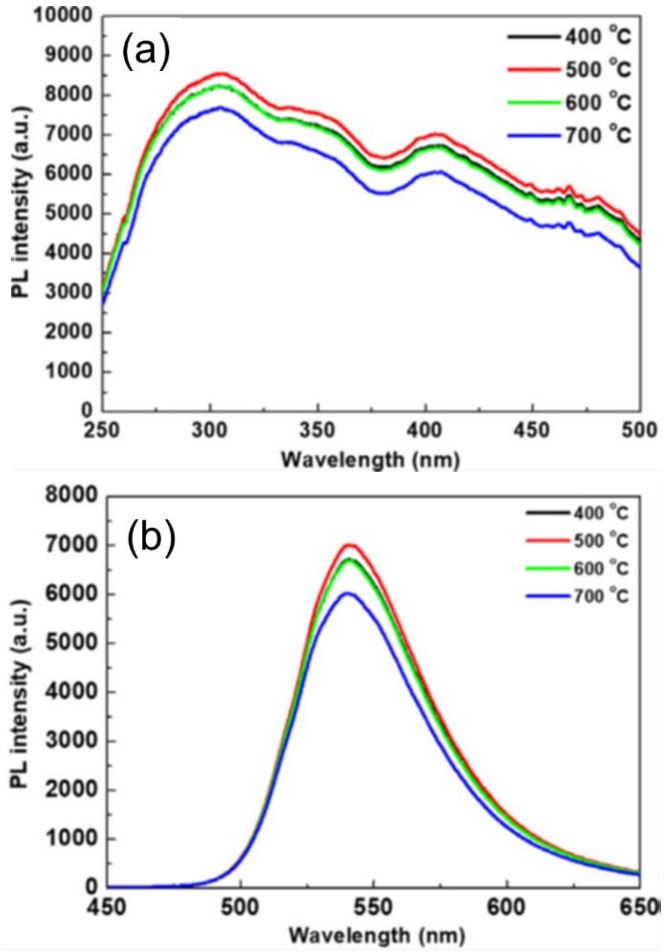

Figure 26. (a) Excitation spectra monitored at 541 nm and (b) Emission spectra under the 365 nm excitation of the TiO_2-coated β-sialon:Eu^{2+} prepared at the temperatures of 400, 500, 600, and 700°C.[72]

The β-sialon:Eu^{2+} phosphor particles were successfully coated by TiO_2 nanoparticles via the sol-gel method. Zhang et al.,[72] the TiO_2-coated β-sialon:Eu^{2+} phosphor had a significantly improved PL performance under the 365 nm excitation, due to the localized surface plasmon resonance (LSPR) at the interface between the TiO_2 coating layer and phosphor surface. It is obviously seen that the TiO_2 coating prepared at TTBO:H_2O = 1:0.5, 1:1, and 1:2 in volume ratio contributed in improving the excitation intensity, by comparing with the as-received phosphor without any coating; whereas, the TiO_2 coating prepared at TTBO:H_2O = 1:4 in volume ratio decreased

the excitation intensity, probably due to the excessive TiO_2 nanoparticles forming a thick layer around the surface of the phosphor particles, as shown in Figure 24a. the emission intensity of the TiO_2-coated powders prepared at TTBO:H_2O = 1:0.5, 1:1, and 1:2 in volume ratio were all improved by 24%, 17%, and 10%, respectively, but was reduced by 42% at TTBO:H_2O = 1:4, by comparing with that of the uncoated sample, as given in Figure 24b. Figure 25 presents the photographs of the (a) β-sialon:Eu^{2+}, (b) TiO_2-coated β-sialon:Eu^{2+} prepared at TTBO:H_2O = 1:0.5 and (c) 1:4 in volume ratio under the 365 nm irradiation. By comparing with the uncoated β-sialon:Eu^{2+}, the coated β-sialon:Eu^{2+} obtained at TTBO:H_2O = 1:0.5 and 1:4 distinctly appeared more luminous and dim brightness, respectively. When the preparation temperature was 500°C, it was responsible for superior PL intensity by considering the important domination factors of higher anatase content and spherical particle shape of the TiO_2 coating layer to the LSPR effect. As shown in Figure 26, the TiO_2-coated β-sialon:Eu^{2+} with TTBO:H_2O = 1:0.5 prepared at 500°C presented the strongest PL intensity, indicating that the temperature is an important factor for preparing the coated samples. To explain the importance of the preparation temperature, it is assumed that the phase transformation and particle growth of the separately synthesized TiO_2 powders discussed above also occurred in the TiO_2 coating layer in the same way. At 500°C, the prepared TiO_2 coating had an estimated anatase composition of ~95 mass%, which is much higher than the coatings fabricated at 600°C (~4 mass%) and 700°C (~3 mass%) As the anatase has higher photocatalytic activity than the rutile,[73–75] it is more feasible for the higher anatase content to produce the photogenerated e- and h+ under the excitation. This favours the reduction of the Ti^{4+} to Ti^{3+} to form the nonstoichiometric TiO_{2-x} nanoparticles responsible for the LSPR effect. On the other hand, it has been reported that the electromagnetic field enhancement significantly depends on the shape and size of the individual particle,[76] and the spherical particle in nano-sized effectively yields the plasmon effect in some metal plasmonic materials.[77, 78] Therefore, it can be understood that the spherical shape with several nanometres for the TiO_2 particles prepared at 500°C effectively produce the LSPR effect very well. However, although the TiO_2 coating prepared at 400°C had a higher anatase content and a smaller spherical particle size than that obtained at 500°C, it played a negative role in the emission intensity of phosphor samples, which is attributable to the low crystallinity of the TiO_2 nanoparticles synthesized at 400°C that impairs the LSPR effect.

Due to the high stability and high transmittance of graphene material, a thin carbon layer was deposited by Yan et al.,[79] on the surface of $SrSi_2O_2N_2$: Eu^{2+} (122) phosphor particles by chemical vapor deposition (CVD) method as to improve its thermal and chemical stability. After coating, the carbon was attached on the phosphor in an amorphous form and alleviated the oxidation of Eu^{2+}, which enhanced the luminous stability and extended the service time of the phosphors. The carbon-coated CVD phosphors better retained luminescence intensity at high temperatures, as shown in Figure 27. The better retaining rate of emission intensity after the carbon coating is due to the decrease of thermal degradation. The carbon coating forms a barrier layer between the phosphor and the outer environment, which effectively suppresses the thermal degradation and greatly improve its thermal stability. In addition, its oxidation resistance and thermal stability of fabricated LED was also improved.

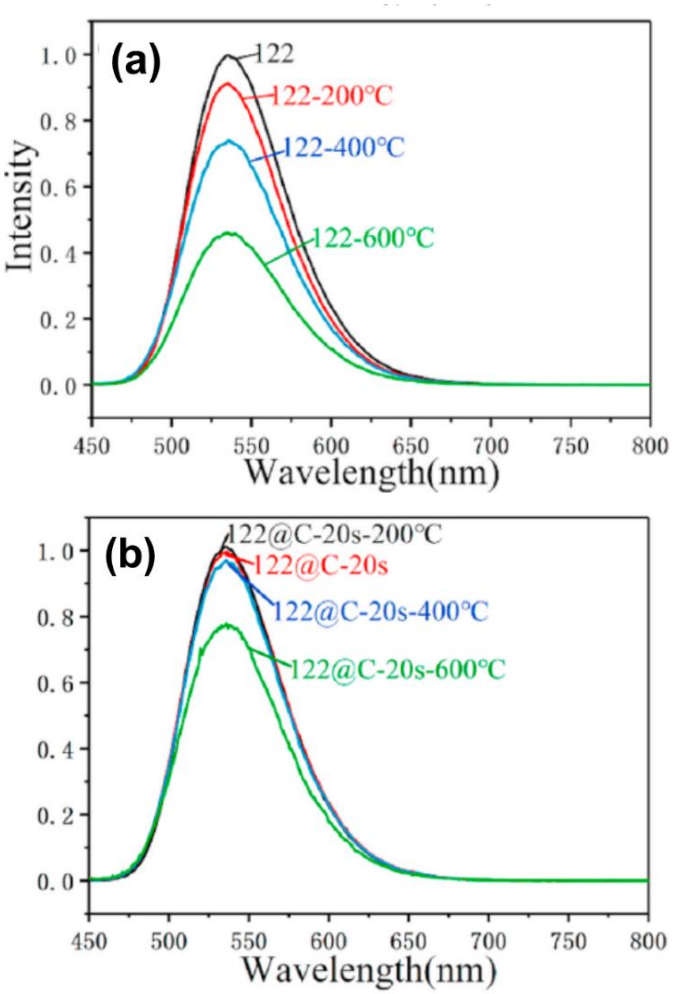

Figure 27. Emission spectra of 122 (d) and 122@C-20s (e) after heat treatment at 200 ◦C, 400 ◦C and 600 ◦C for 2 h in air.[79]

Due to the high transmittance and high chemical inertness of graphene, it was coated on the surface of $Sr_2Si_5N_8$: Eu^{2+} phosphor at single layer coating by chemical vapor deposition, aiming to improve its thermal stability and hydrolysis resistance (Figure 28a), as reported by Liu et al.[80] In coated $Sr_2Si_5N_8$:Eu^{2+} phosphor, the oxidation degree of Eu^{2+} to Eu^{3+} was significantly suppressed. At the same time, the surface of $Sr_2Si_5N_8$:Eu^{2+} particle turned from hydrophilic to hydrophobic after carbon coating (Figure 28b), and the carbon coated $Sr_2Si_5N_8$:Eu^{2+} phosphor maintained about 95% of its initial luminous intensity as compared with 35% of the uncoated due to improved hydrolysis resistance, after tests at 85 ◦C and 85% humidity for 200 h. By observing the *in-situ* microstructure evolution of coated phosphor in air-water vapor environment, remained presence of the carbon layer even at 500 ◦C explained the excellent chemical stability of carbon coated $Sr_2Si_5N_8$:Eu^{2+} phosphor in complex environment (Figure 28c). Yang et al.,[81] coated $Sr_2Si_5N_8$:Eu^{2+} phosphor by an ultrathin carbon layer by chemical vapor deposition and further annealed carbon-coated powders in N_2 atmosphere at a high temperature to trigger the carbothermal reaction. the

carbothermal reaction resulted in the removal of oxygen in the phosphor particle by a part of the carbon on the surface. On the other hand, the remaining carbon crystallized, forming a graphene-like multilayer that protected the phosphor particle from the penetration of the external oxygen, as shown in Figure 29.

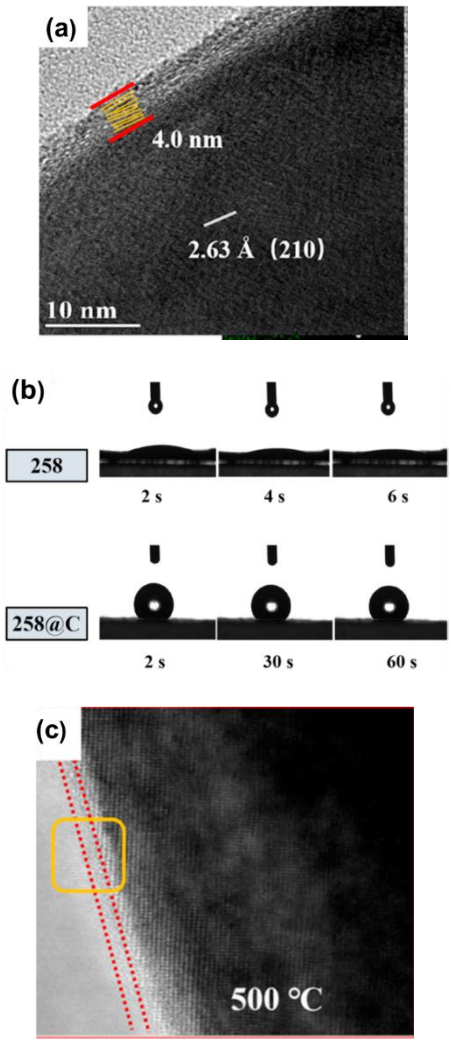

Figure 28. (a) HRTEM images of $Sr_2Si_5N_8:Eu^{2+}$@C-600 phosphor at heat treatment 700 ◦C, (b) contact angle tests of $Sr_2Si_5N_8:Eu^{2+}$ and $Sr_2Si_5N_8:Eu^{2+}$@C-600 phosphors, and (c) In-situ HRTEM images of $Sr_2Si_5N_8:Eu^{2+}$@C-600 phosphor at 500 ◦C.[80]

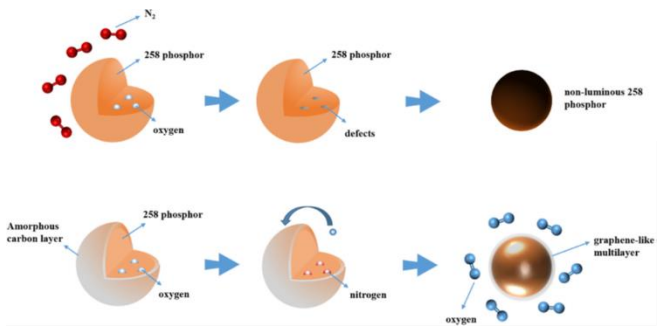

Figure 29. A proposed mechanism of thermal degradation of $Sr_2Si_5N_8:Eu^{2+}$ and $Sr_2Si_5N_8:Eu^{2+}$@C-A phosphors after heat treatment in nitrogen.[81]

In order to shed light on the degradation mechanism, a novel mechanism for the thermal degradation of $Sr_2Si_5N_8:Eu^{2+}$ phosphors was analysed by Yang et al.[82] After heat-treatment in N_2, the bonds between Si atom and O impurity inside the crystal lattice became unstable, resulting in their detachment and in formation of local nano-defects. $SrSiO_3$ precipitated on the surface of the phosphor particles, which led to the destruction of the original lattice structure and to the formation of deep defect energy levels, and, as a result, caused a decrease in the luminous intensity of the phosphor. That is, the detachment of active Si and O impurity led to the formation of Si-O vacancies, favouring the shrinkage of the crystal lattice. Si-O vacancies, which are related to deep defect energy levels, were generated in the crystal lattice. It means higher temperature led to the formation of structural defects caused a higher probability of non-radiative relaxation, for decreasing in luminescence intensity.

Other strategies to improve stability for phosphors

Phosphor in glass have been reported to be used as matrix embedding phosphor particles, with high thermal conductivity and superior chemical stability. Moreover, phosphor in glass provides some advantages of easy preparation, variable shape, and easy mass production, benefiting its promising application for high-power LED lighting.[83–87] Especially, embedding quantum dots (QDs), include IIB-VIA, IVB-VIA, and halide perovskite, into inorganic glass can secure chemical, thermal, and mechanical stabilities by overcoming instability bottleneck, thus providing access to device manufacturing and endurable application.[88–90]

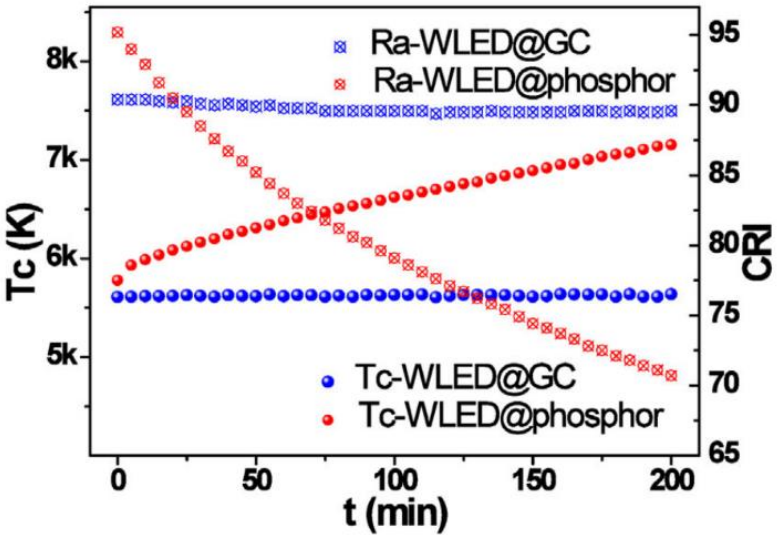

Figure 30. Stability comparison of related CCT and CRI of WLED@GC and WLED@phophor.[91]

Li et al.,[91] designed a strategy of in-situ glass crystallization combining with Eu^{2+} for fabricating Eu^{2+}-doped $NaAlSiO_4$ (NASO) glass ceramic (GC) composites. The doped Eu^{2+} dopants were accommodated into crystalline lattice without the requirement of

long-distance ionic diffusion, providing strong crystal-field environment for 5d-4f transition of Eu^{2+}. The fabricated GC composites produce intense greenish-yellow emission with apparent photoluminescence quantum yield (PLQY) of ≈70%, intrinsic PLQY of ≈100%, superior thermal stability with 90% PL remained at 150 °C and excellent water-resistance. Impressively, the related CCT and CRI parameters of the WLED@GC device remained in a steady state, on the contrary, CCT rose from initial 5778 to 7157 K and CRI decreased from 95.2 to 70.7 within 200 min of the WLED@phosphor, as demonstrated in Figure 30. Employing NSAO: Eu^{2+} GC as a colour converter, the performance of constructed LED/laser diode (LD) lighting devices is extraordinary and stable during long-term working, therefore opening up new avenues for exploring novel glass ceramic materials used in LED application.

Perovskite quantum dots (PeQDs) have been regarded as an alternative to traditional phosphor colour converters in the backlit display due to their improved colour gamut and rendition of LCD. However, the pending barriers of aggregation quenching and structure instability are hindering their practical applications. To solve this problem, recently, high-quality CsPbX3(X = Br, Br/I) PeQDs were in situ precipitated inside glass to produce nanocomposites with superior optical performance and stability were reported by Lin et al.[92] In this work, the highest photoluminescence quantum yield (PLQY) of ~100% for CsPbBr3@glass is ascribed to the elimination of the inner filter effect via a physical dilution approach to restore its apparent value to an intrinsic one (Figure 31a). And the exceptional photostability and water/heat resistance are benefited from their effective isolation from the external environment by the surrounding glass network units (Figures 31b and 31c). Finally, PeQDs@glass@PDMS monolithic film was employed to assemble a high-performance backlit LCD, and its colour gamut reached 152% of commercial LCD and 103% of NTSC (Figures 31d and 31e). Liao et al,.[93] reported that a hierarchical structure quantum dots-in-glass film (QiGF) was fabricated via co-sintering stable green/red-emitting CsPbX3@glass (X3 = Br3, Br1.5I1.5) and commercial low-melting glass on the sapphire substrate. A brand-new white-lighting source designed by coupling a blue laser with a pattern "QiGF wheel" produced ultra-narrow blue/green/red tri-colour emissions and total luminous flux of 146 lm, showing more natural and real colour restoration for its wide colour gamut display feature (157% of conventional light-emitting diode projection and 107% of NTSC standard). As showing in Figure 32, EL spectra of (Figure 32a) commercial LED and (Figure 32b) the prototype laser-driven light source, the mixture of blue, green, and green tri-colours produces bright white light in a pattern "QiGF wheel" (Figure 32c). The photographs of projection display based on two different light sources are comparably presented in Figures 32d−32g. According to the calculated CIE colour coordinates, the colour gamut of the "QiGF wheel" based projector reaches 107% of NTSC standard and 157% of that of the commercial LED based projector (Figure 32h). This highlights the practical application of CsPbX3 quantum dots composite as an efficient laser-driven colour converter in projection display with achieving wide-colour-gamut and high-quality image presentation. Chen et al,.[94] prepared amorphous-glass-protected green/red CsPbX3 quantum dots (QDs) by elaborately optimizing glass structure, perovskite concentration, and in situ crystallization (Figure 33a), with PLQYs of green CsPbBr3@glass and red CsPbBr1.5I1.5@glass as 94% and 78%, respectively. CsPbX3@glass can endure harsh commercial standard aging tests of 85 °C/85%RH and blue-light-irradiation (Figures 33b and 33c), due to complete isolation of QDs from external environment by glass network, The perovskite WLED arrays-based backlit unit and a prototype display device showed more vivid and wide-colour-gamut feature, indicating practical application of CsPbX3@glass composite as an efficient and stable light colour converter in backlit display.

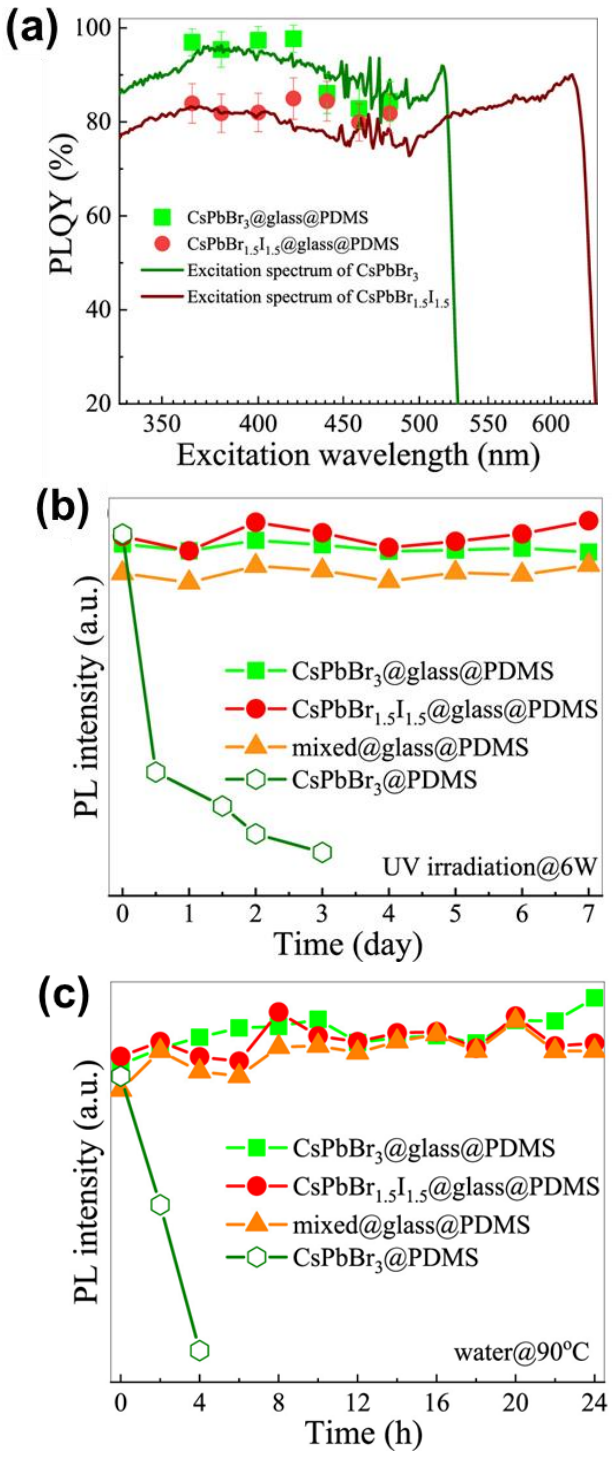

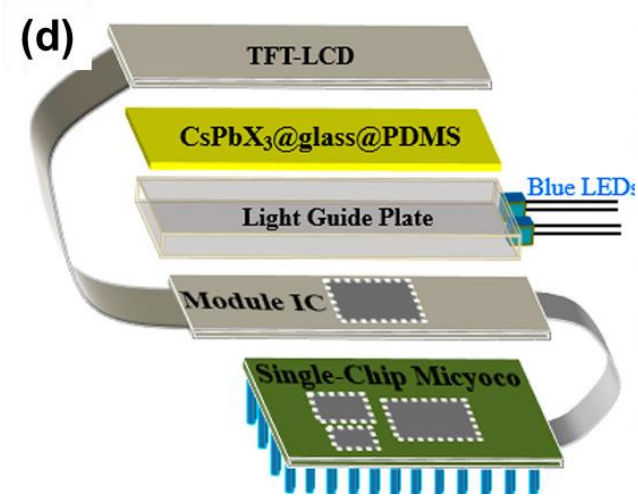

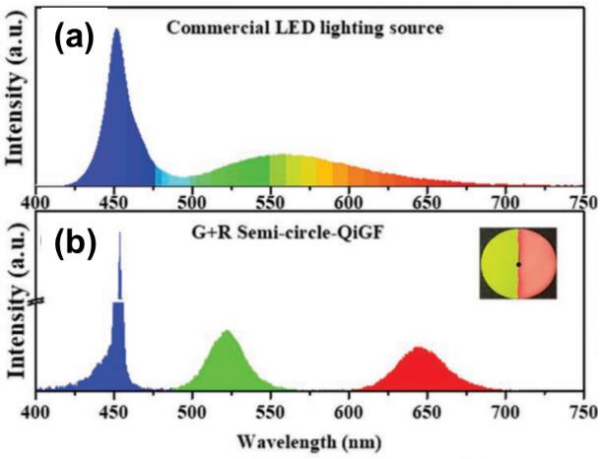

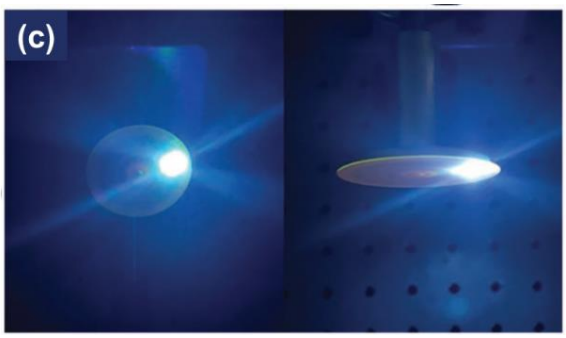

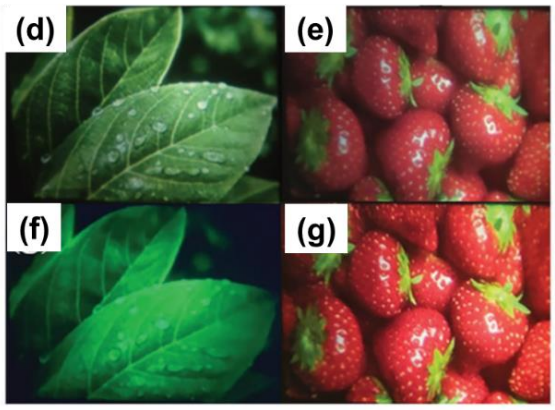

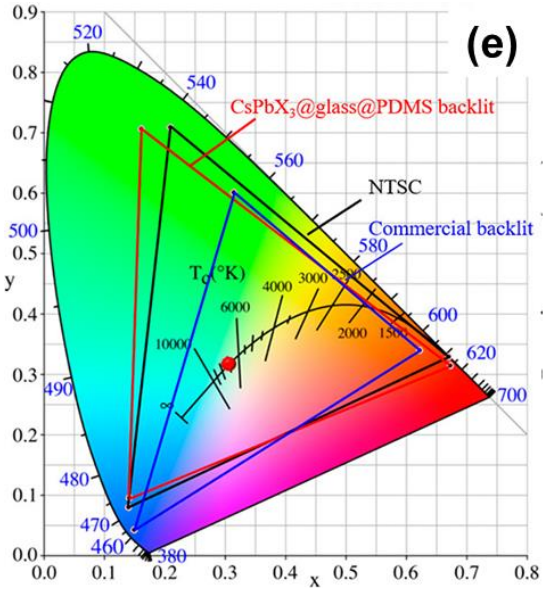

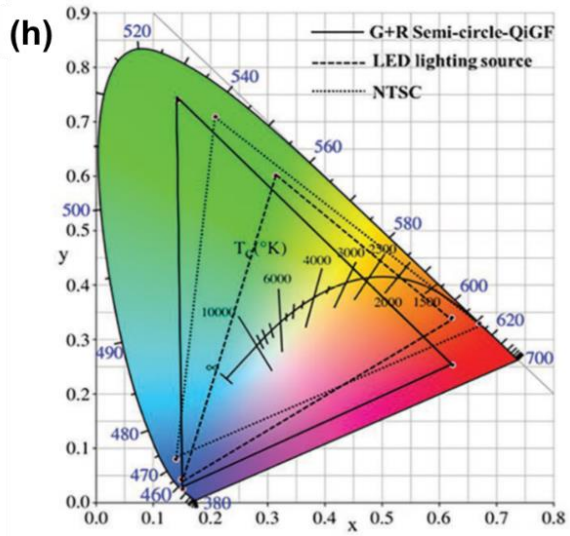

Figure 31. (a) Dependence of PLQYs for the CsPbBr3@glass@ polydimethylsiloxane (PDMS) and CsPbBr1.5I1.5@glass@PDMS films on the wavelength of incident excitation light. The excitation spectral lines are provided as the guides, (b) Photostability test under UV light (6W) irradiation for 7 days, (c) Humidity-resistance test under the strengthening condition by directly immersing CsPbX3@glass@PDMS films in water maintained at 90 °C for 24 h, (d) schematic illustration of LCD device structure using the as-prepared backlight unit. Display performance of LCD screen, and (e) colour gamut of the commercial screen (blue line), the $CsPbX_3$@glass@PDMS film screen (red line) and NSTC 1953 standard (black line) in the CIE diagram.[92]

Figure 32. Electroluminescent (EL) spectra of (a) commercial LED and (b) the prototype laser-driven light source. (c) Luminescent photos of a pattern "QiGF wheel" with green & red semi-circles irradiated by blue laser when rotating at 3000 rpm. Projection display performance of (d) and (e) LED-based projector and (f) and (g) QiGF-converted laser-driven projector, and (h) CIE diagram showing NTSC standard and the colour gamut of the prototype laser-driven projector and LED-based projector.[93]

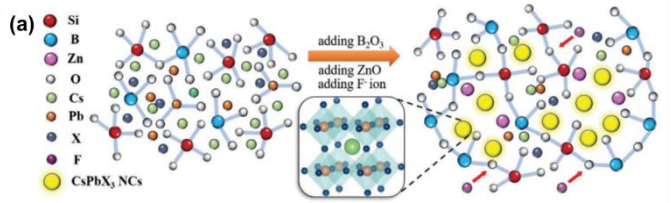

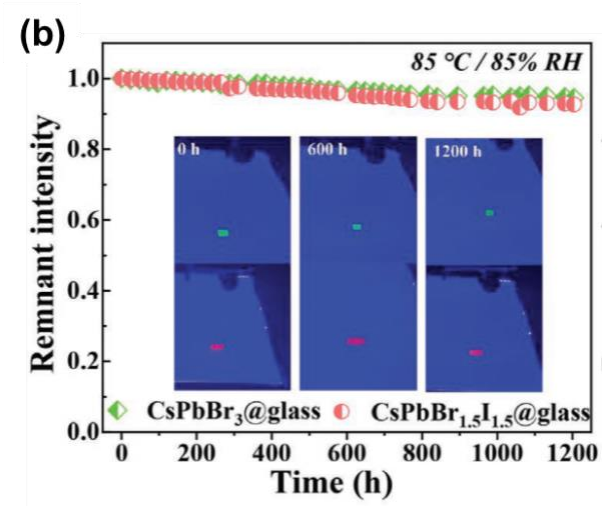

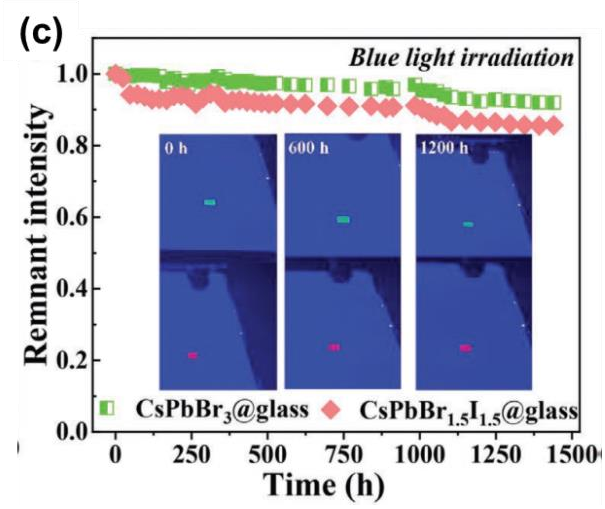

Figure 33. (a) Schematic illustration of SiO2-B2O3-ZnO-CaF2 glass network structure and in-situ growth of CsPbX3 PeQDs, (b) Heat/humidity resistance test of CsPbX3@glass under accelerated aging condition at 85 °C/85%RH, and (c) photostability test under blue light (optical power: 40W m-2) irradiation for 60 days. Insets are illuminated photographs of the corresponding samples after stability tests.[94]

Summary and outlook

Recent developments about the modifications upon particle surface by using various surface modification technologies are reviewed for some typical phosphors suitably used in LEDs. For the fluorides-and sulphides-based phosphors, the surface protective layer effectively protected them from moisture; for the silicates-and oxides-based phosphors, the surface coating dramatically improved their PL efficiencies; for the nitrides-and oxynitrides-phosphors, the surface passivation treatment significantly reduced their thermal degradation about PL property. In this case, the surface modification for the phosphors would be potentially expected for applying in high-efficiency and high-stability LEDs. In addition, embedding phosphors in inorganic glass matrix, especially for QDs, were also revealed as an effective method to improve phosphor stability for LED applications. In the near future, with the increasing demand in energy-efficient lighting market, LEDs will accelerate to replace conventional lamps. As a result, the development of innovative surface modification technology, not limited in the methods review above, is prospective as a more effective and less cost way, opening up new possibilities for improving performance and functionality in a variety of the phosphors used in LEDs.

Acknowledgements

This work was partly supported by JST CREST Gant Number JPMJCR19J2, Japan.

Notes and references

1. A. D. Almeida, B. Santos, B. Paolo and M. Quicheron, *Renew. Sust. Energ. Rev.*, 2014, **34**, 30–48.
2. R. J. Xie and N. Hirosaki, *Sci. technol. Adv. Mater.,* 2007, **8**, 588–600.
3. R.-J. Xie, Y. Li, N. Hirosaki and H. Yamamoto, Nitride Phosphors and Solid-State Lighting. CRC Press, New York, USA, 2011.
4. C. Lin and R. S. Liu, *J. Phys. Chem. Lett.,* 2011, **2**, 1268–1277.
5. R. Verstraete, G. Rampelberg, H. Rijckaert, I. V. Driessche, E. Coetsee, M. M. Duvenhage, P. F. Smet, C. Detavernier, H. Swart and D. Poelman, *Chem. Mater.,* 2019, **31**, 7192–7202.
6. P. F. Smet, I. Moreels, Z. Hens and D. Poelman, *Materials*, 2010, **3**, 2834–2883.
7. G. B. Nair and S. J. Dhoble, Phosphors Synthesis and Applications. CRC Press, New York, USA, 2018.
8. Z. Xia, Z. Xu, M. Chen and Q. Liu, *Dalton Trans.,* 2016, **45**, 1121411232.
9. D. Singh, S. Sheoran and V. Tanwar, *Adv. Mater. Lett.*, 2017, **8**, 656–672.
10. I. Gupta, S. Singh, S. Bhagwan and D. Singh, *Ceram. Int.*, 2021, **47**, 19282–19303.
11. N. C. George, K. A. Denault and R. Seshadri, *Annu. Rev. Mater. Res.*, 2013, **43**, 481–501.

12. R. J. Xie, N. Hirosaki, Y. Li and T. Takeda, *Materials*, 2010, **3**, 3777–3793.
13. J. Tian and W. Zhuang, *Inorg. Chem. Front.*, 2021, **8**, 4933–4954.
14. T. Takeda, R. J. Xie, T. Suehiro and N. Hirosaki, *Prog. Solid State Chem.*, 2018, **51**, 41–51.
15. Y. Y. Zhou, E. H. Song, T. T. Deng and Q. Y. Zhang, *ACS Appl. Mater. Interfaces,* 2018, **10**, 880−889.
16. Y. Zhou, E. Song, T. Deng, Y. Wang, Z. Xia, Q. Zhang, *Adv. Mater. Interfaces,* 2019, **6**, 1802006.
17. C. Jiang, M. G. Brik, A. Srivastava, L. Li, M. Peng, *J. Mater. Chem. C,* 2019, **7**, 247−255.
18. T. Takahashi and S. Adachi, *J. Electrochem. Soc.,* 2008, **155**, E183−E188.
19. Y. Jin, M. H. Fang, M. Grinberg, S. Mahlik, T. Lesniewski, M. G. Brik, G. Y. Luo, J. Lin, R.S. Liu, *ACS Appl. Mater. Interfaces,* 2016, **8**, 11194−11203.
20. Y. Xu and S. Adachi, *J. Appl. Phys.,* 2009, **105**, 013525.
21. Y. Xu and S. Adachi, *J. Electrochem. Soc.,* 2011, **158**, J58−J65.
22. L. Huang, Y. Zhu, X. Zhang, R. Zou, F. Pan, J. Wang and M. Wu, *Chem. Mater.,* 2016, **28**, 1495−1502.
23. L. Wang; E. Song, Y. Zhou, T. Deng, S. Ye and Q. Zhang, *J. Mater. Chem. C,* 2017, **5**, 7253−7261.
24. J. Moon, B. Min, S. Jin, M. Jang, M. Kang, K. Han and J. Yoo, *Opt. Mater. Express,* 2016, **6**, 782−792.
25. P. Arunkumar, Y. Kim, H. Kim, S. Unithrattil, and W. Im, *ACS App. Mater. Interfaces,* 2017, **9**, 7232−7240.
26. M. H. Fang, C. S. Hsu, C. Su, W. Liu, Y. H. Wang and R. S. Liu, *ACS App. Mater. Interfaces,* 2018, **10**, 29233–29237.
27. Y. X. Liu, J. X. Hu, L. C. Ju, C. Cai, V. B. Hao, S. H. Zhang, Z. W. Zhang, X. Xu, X. Jian, L. J. Yin, *Ceram. Int.,* 2020, **46**, 8811–8818.
28. H. Yu, B. Wang, X. Bu, Y.G. Liu, J. Chen, Z. Huang and M. Fang, *Ceram. Int.,* 2020, **46**, 18281–18286.
29. D. Deng, J. Qiang, T. Wang, J. Lei, L. Wang, Y. Li, S. Liao and Y. Huang. *J. Lumin.,* 2022, **252**, 119429.
30. J. Zhou, Y. Wang, Y. Chen, Y. Zhou, B. Milićević, L. Zhou, J. Yan, J. Shi, R.-S. Liu and M. Wu, *Angew. Chem. Int. Ed.,* 2021, **60**, 3940.
31. D. Huang, H. Zhu, Z. Deng, Q. Zou, H. Lu, X. Yi, W. Guo, C. Lu and X. Chen, *Angew. Chem. Int. Ed.,* 2019, **58**, 3843.
32. W. T. Huang, Y. Meesala, H. P. Hsueh, M. H. Fang, Z. Bao, J. W. Chiou, R.S. Liu, *Chem. Eng. J.,* 2022, **430**, 132789.
33. Z. Fang, X. Lai, J. Zhang and R. Zhang, *Int. J. Appl. Ceram. Technol.,* 2021, **18**, 1106–1113.
34. J. Qiang, L. Wang, T. Wang, Y. Yu, D. Deng, C. Wu, S. Liao and S. Li, *Ceram. Int.,* 2022, **48**, 17253–17260.
35. L. Huang, Y. Liu, S. Si, M. G. Brik, C. Wang, and J. Wang. *Chem. Commun.,* 2018, **54**, 11857–11860.
36. L. Huang, Y. Zhu, X. Zhang, R. Zou, F. Pan, J. Wang and M. Wu, *Chem. Mater.,* 2016 **28**, 1495–1502.
37. Y. Zhao, Q. Guan, H. Wang, Y. Li, J. Lu and R.-J. Xie. *J. Mater. Chem. C,* 2022,**10**, 9867–9874.
38. J. Moon, B. Min, J. Kim, M. Jang, K. Ok, K. Y. Han and J. Yoo, *Opt. Mater. Express,* 2016, **6**, 782–792.
39. R. Verstraete, H. F. Sijbom, J. J. Joos, K. Korthout, D. Poelman, C. Detavernier and P. F. Smet, *ACS Appl. Mater. Interfaces,* 2018, **10**, 18845.
40. D. Poelman, J. V. Haecke and P. F. Smet, *J. Mater. Sci. Mater. Electron.,* 2009, **20**, 134–138.
41. I. Park, J. Kim, J. Yoo, H. Shin, C. Kim and C. Choi. *J. Electrochem. Soc.,* 2008, **155**, J132–J135.
42. Nursen. Avci, I. Cimieri, P. F. Smet and D. Poelman, *Opt. Mater.,* 2011, **33**, 1032–1035.
43. S. H. Yoo and C. K. Kim. *J. Electrochem. Soc.,* 2009, **156**, J170–J173.
44. J. Park, K. Choi, H. Kang, J. Kim and C. Kim. *Electrochem. solid-state lett.,* 2007, **10**, J15–J18.
45. M. Zhao, Q. Zhang and Z. Xia, *Acc. Mater. Res.,* 2020, **1**, 137–145.
46. L. Fernández-Rodríguez, A. Durán and M.J. Pascual. *Open Ceram.,* 2021, **7**, 1–20.
47. H. Lee and J. Yoo, *Appl. Surf. Sci.,* 2011, **257**, 8355–8359.
48. J. Yi, C. Bernard, F. Variola, S. Zalzal, J. Wuest, F. Rosei and A. Nanci, *Surf. Sci.,* 2006, **600**, 4613–4621.
49. M. Zhao, K. Cao, M. Liu, J. Zhang, R. Chen, Q. Zhang and Z. Xia, *Angew. Chem. Int. Ed.,* 2020, **59**, 12938–12943.
50. R. Chen, K. Qu, J. Li, P. Zhu, C. Duan, J. Zhang, X. Li, X. Liu and Z. Yang, *ACS Appl. Nano Mater.,* 2018, **1**, 5500–5506.
51. H. Wang, Y. Liu, H. Liu, Z. Chen, P. Xiong, X. Xu, F. Chen, K. Li and Y. Duan, *Adv. Mater. Interfaces,* 2018, **5**, 1701248.
52. Q. Dai, M. E. Foley, C. J. Breshike, A. Lita and G F. Strouse, *J. Am. Chem. Soc.,* 2011, **133**, 15475-15486.
53. T. Schlieper, W. Milius and W. Schnick, *Z. Anorg. Allg. Chem.,* 1995, **621**, 1380–1384.
54. Y. Li, J. V. Steen, J. V. Krevel, G. Botty, A. Delsing, F. D. With, G. DiSalvo and H. Hintzen, *J. Alloys Compd.,* 2006, **417**, 273–279.
55. R. J. Xie, N. Hirosaki, T. Suehiro, F. Xu and M. Mitomo, *Chem. Mater.,* 2006, **18**, 5578–5583.
56. R.J. Xie, N. Hirosaki, T. Takeda and T. Suehiro, *ECS J. Solid State Sci. Technol.,* 2013, **2**, R3031–R3040.
57. C. Chi, P. Chen, Y. L. Lee, I. Liu, S. C. Chou, X. L. Zhang and U. Bach, *J. Mater. Chem.,* 2011, **21**, 17534–17540.
58. D. Wang, S. Hou, H. Wu, C. Zhang, Z. Chu and D. Zou, *J. Mater. Chem.,* 2011, **21**, 6383–6388.
59. F. Wang, X. Zhang, L. Wang, Y. Jiang, C. Wei, J. Sun and Y. Zhao, *ACS Appl. Mater. Interfaces,* 2014, **6**, 15098–15104.
60. C. Zhang, T. Uchikoshi, R. J. Xie, L. Liu, Y. Cho, Y. Sakka, N. Hirosaki and T. Sekiguch, *J. Mater. Chem. C,* 2015, **3**, 7642–7651.
61. C. Zhang, T. Uchikoshi, R. J. Xie, L. Liu, Y. Cho, Y. Sakka, N. Hirosaki and T. Sekiguchi, *Phys. Chem. Chem. Phys.,* 2016, **18**, 12494–12504.
62. H. Yamamoto, S. Shionoya and W. M. Yen, Phosphor Handbook. CRC press, New York, USA, 2006.
63. K. B. Kim, K. W. Koo, T. Y. Cho and H. G. Chun, *Mater. Chem. Phys.,* 2003, **80**, 682–689.
64. R.J. Xie, N. Hirosaki, N. Kimura, K. Sakuma and M. Mitomo, *Appl. Phys. Lett.,* 2007, **90**, 191101.
65. Y. Zhao, L. Yin, O. ten Kate, B. Dierre, R. Abellon, R. J. Xie, J. van Ommen and H. intzen, *J. Mater. Chem. C,* 2019,**7**, 5772–5781.
66. J. Seo, S. Lee, H. Moon, S. Han and S. Sohn, *Mol. Cryst. Liq. Cryst.,* 2010, **531**, 82–89.
67. Z. Chen, Y. Yan, J. Liu, Y. Yin, H. Wen, G. Liao, C. Wu, L. Zao, D. Liu, H. Tian, C. Zhang and S. Li, *J. Alloy. Comp.,* 2009, **478**, 679–683.
68. L. Bergstrom and E. Bostedt, *Colloid. Surface.,* 1990, **49**, 183–197.
69. E. Liden, L. Bergstrom, M. Persson and R. Carlsson, *J. Eur. Ceram. Soc.,* 1991, **7**, 361–368.

70. C. Zhang, T. Uchikoshi, T. Kitabatake, Y. Sakka and N. Hirosaki, *Appl. Surf. Sc.,* 2013, **280**, 229– 234.
71. C. Zhang, T. Uchikoshi, R. J. Xie, L. Liu, Y. Sakka and N. Hirosaki, *J. Alloy. Compd.,* 2018, **741**, 454–458.
72. C. Zhang, T. Uchikoshi, R. J. Xie, L. Liu, Y. Sakka and N. Hirosaki, *J Am Ceram Soc.,* 2019, **102**, 294–302.
73. K. Tanaka, M. F. V. Capule and T. Hisanaga, *Chem Phys Lett.,* 1991, **187**, 73–76.
74. R. I. Bickley, T. Gonzalezcarreno, J. S. Lees, L. Palmisano and R. J. D. Tilley, *J Solid State Chem.,* 1991, **92**, 78–90.
75. H. Luo, T. Takata, Y. Lee, J. Zhao, K. Domen and Y. Yan, *Chem Mater.,* 2004, **16**, 846–849.
76. V. M. Shalaev, Nonlinear optics of random media. Berlin, Germany: Springer, 2000.
77. P. Mulvaney, *Langmuir,* 1996, **12**, 788–800.
78. K. P. Charle, W. Schulze and B. Winter, *Z. Phys. D. Atoms. Mol. Clusters,* 1989, **12**, 471–475.
79. R. Yan, H. Ding, L. Gao, D. Chen, L. Yin, A. Xu, H. Lv, X. Xu, L. Ju and L. Yin, *Mater. Chemi. Phys.,* 2020, **256,** 123759.
80. Y. Liu, H. Wang, D. Chen, L. Gao, X. Wang, X. Jian, C. Mu, X. Xu and L. Yin, Ceram. Int., 2021, 47, 3244−3251.
81. X. Yang, X. Xing, Y. Zhao, Z. Yang, Y. Liu, C. Mu, H. V. Bui, Z. Zhang, S. Agathopoulos, X. Xin and L. Yin, Ceram. Int., 2023, 49, 20159−20167.
82. X. Yang, X. Xing, Y. Liu, C. Mu, H. V. Bui, Z. Zhang, S. Agathopoulos, X. Xin and L. Yin, Opt. Mater., 2021, 121, 111506.
83. R. Zhang, H. Lin, Y. Yu, D. Chen, J. Xu and Y. Wang, Laser Photonics Rev., 2014, 8, 158−164.
84. J. Deng, H. Zhang, X. Zhang, Y. Zheng, J. Yuan, H. Liu, Y. Liu, B. Lei and J. Qiu, J. Mater. Chem. C, 2018, 6, 1738−1745.
85. J. Yu, S. Si, Y. Liu, X. Zhang, Y. Cho, Z. Tian, R.-J. Xie, H. Zhang, R. Li and J. Wang, J. Mater. Chem. C, 2018, 6, 8212−8218.
86. D. Zhang, W. Xiao, C. Liu, X. Liu, J. Ren, B. Xu and J. Qiu, Nat. Commun., 2020, 11, 2805.
87. P. Huang, Y. Zhao, J. Wang, Y. Zheng, P. Yang, Q. Zheng, S. Gu, B. Zhou, W. Jiang and L. Wang, J. Am. Ceram. Soc., 2020, 103, 4989−4998.
88. M. Xia, J. Luo, C. Chen, H. Liu and J. Tang, Adv. Opt. Mater., 2019, 7, 1900851.
89. D. Chen, S. Yuan, X. Chen, J. Li, Q. Mao, X. Li and J. Zhong, J. Mater. Chem. C, 2018, 6, 6832−6839.,
90. B. Yang, F. Zheng, S. Mei, Z. Chen, Y. Xie, H. Dai, X. Wei, W. Zhang, F. Xie, J. Ju, Y. Chu, J. Zhou and R. Guo, Appl. Surf. Sci., 2020, 512, 145655.
91. X. Li, C. Yang, L. Qiu, S. Wang, Y. Chen, M. Yin and D. Chen, Laser Photonics Rev., 2022, 16, 2100346.
92. S. Liao, Z. Yang, J. Lin, S. Wang, J. Zhu, S. Chen, F. Huang, Y. Zheng and D. Chen, Adv. Funct. Mater., 2023, 33, 2210558.
93. J. Lin, Y. Lu, X. Li, F. Huang, C. Yang, M. Liu, N. Jiang and Chen, D. ACS Energy Lett., 2021, 6, 519−528.
94. S. Chen, J. Lin, S. Zheng, Y. Zheng and D. Chen, (2023). Adv. Funct. Mater., 2023, 2213442.